

Combining Pati-Salam and Flavour Symmetries

Thorsten Feldmann^{*}, Florian Hartmann[†],
Wolfgang Kilian[‡], Christoph Luhn[§]

*Theoretische Physik 1, Naturwissenschaftlich-Technische Fakultät,
Universität Siegen, 57068 Siegen, Germany*

June 3, 2015

Abstract

We construct an extension of the Standard Model (SM) which is based on grand unification with Pati-Salam symmetry. The setup is supplemented with the idea of spontaneous flavour symmetry breaking which is mediated through flavon fields with renormalizable couplings to new heavy fermions. While we argue that the new gauge bosons in this approach can be sufficiently heavy to be irrelevant at low energies, the fermionic partners of the SM quarks, in particular those for the third generation, can be relatively light and provide new sources of flavour violation. The size of the effects is constrained by the observed values of the SM Yukawa matrices, but in a way that is different from the standard minimal-flavour violation approach. We determine characteristic deviations from the SM that could eventually be observed in future precision measurements.

^{*}E-mail: thorsten.feldmann@uni-siegen.de

[†]E-mail: hartmann@physik.uni-siegen.de

[‡]E-mail: kilian@physik.uni-siegen.de

[§]E-mail: christoph.luhn@uni-siegen.de

1 Introduction

Grand Unified Theories (GUTs) represent an attractive direction to search for extensions of the Standard Model (SM) of particle physics (see e.g. [1]). The peculiar structure of the SM gauge group and its fermionic representations observed at low energies finds a more natural-looking explanation when embedded into larger (but simpler) groups that may be realized at higher energies. In particular, each generation of SM quarks and leptons fits into a 16-dimensional spinor representation of the group $SO(10)$ [2] which then also contains a right-chiral neutrino that can be used to explain the tiny but non-vanishing neutrino masses via the seesaw mechanism [3–6]. Theoretical complication re-enters when it comes to the question of how the GUT symmetry is broken down to the $SU(3) \times SU(2) \times U(1)$ symmetry of the SM. Different Higgs representations of the GUT group can be chosen, and the symmetry breaking further depends on the parameters controlling the ground state of the scalar potential. It turns out that the SM group can be reached from $SO(10)$ via basically two separate routes: either via the Georgi-Glashow group $SU(5)$ [7], or via the Pati-Salam (PS) group $SU(4) \times SU(2) \times SU(2)'$ [8, 9].

Adopting a non-supersymmetric framework, we will focus on the PS gauge group with an explicit Z_2 symmetry relating the couplings and representations of the two $SU(2)$ group factors (which affect the left- and right-chiral SM fermions, respectively). Recent work in this framework [10–17] suggests that it is worthwhile to consider PS scenarios with an extended field content (as compared to minimal setups) where the breaking from the PS group to the SM group involves several distinct mass scales which eventually realize gauge-coupling unification at the GUT scale. Here we investigate a particular construction which also allows us to address questions relating to flavour and flavour mixing.

The idea of combining grand unification with flavour is itself not new (for reviews see e.g. [18–23]). The intimate connection of the SM fermions, which is dictated by the GUT multiplet structure, generally relates the Yukawa matrices of different sectors in an unrealistic way. In order to accommodate the observed Yukawa structures, it is therefore necessary to introduce more than one GUT-breaking Higgs field [24, 25]. Flavour symmetries are then imposed to control the resulting Yukawa patterns by suitably chosen vacuum expectation values (VEVs) of scalar flavon fields. Typically, the so-constructed Yukawa matrices arise as sums of mostly non-renormalizable terms [26–28]. For explicit constructions compatible with the PS gauge group, see e.g. [29–38].

In contrast to this traditional approach, we implement an idea first proposed by Grinstein, Redi and Villadoro (GRV) in [39], where the concept of gauged flavour symmetries is realized within a renormalizable field theory. Among others, this requires to introduce new heavy partners for the SM fermions in order to cancel gauge anomalies associated with the chiral representations of the flavour symmetry group (see also [40]). The new fermions can then be used to mediate flavour-symmetry breaking — which is realized by VEVs of new matrix-valued scalar flavon fields¹ — to the SM sector. The original GRV paper focused on the SM quark multiplets. With a minimal set of new fermions and scalars, the authors have shown that the SM Yukawa matrices $Y_{u,d}$ for up- and down-type

¹The possibility of obtaining hierarchical structures for flavon VEVs (and thus realizing sequential flavour-symmetry breaking as described in [41]) by an appropriate flavour-invariant potential has been discussed, for instance, in [42–50].

quarks are effectively given by the inverse of the corresponding flavon VEVs. Here, the partner of the top quark t' plays a special role: the large Yukawa coupling of the top quark implies that t' can be relatively light (i.e. within the reach of direct searches at the LHC at CERN), and that it can have a substantial mixing with the SM top quark. This leads to interesting new physics effects in electroweak precision observables and flavour transitions involving the third generation of quarks. At the same time, indirect flavour bounds from the first and second generation (most notably from $K - \bar{K}$ mixing and rare kaon decays) are naturally satisfied (see also [51]). Variants of the GRV idea in the context of the SM [52], GUTs [53–55], and supersymmetric theories [56, 57] have also been discussed in the literature.

The new essential ingredients in this work are a consequence of embedding the GRV mechanism in an explicit left-right (i.e. Z_2) symmetric PS GUT with a Higgs bi-doublet. First, this requires to introduce (at least) two partners for each conventional PS fermion multiplet. Second, in order to obtain realistic masses and mixing for quarks and leptons, one has to introduce different types of flavon fields. In the minimal setup that we will construct for the quark sector, we consider flavons that transform as singlets and triplets under the $SU(2)$ factors of the PS symmetry group. The breaking of the flavour symmetry by the singlet VEV alone treats up- and down-type quarks in the same way, such that the corresponding Yukawa matrices are identical, $Y_u = Y_d$. An additional VEV for the $SU(2)'$ triplet flavon then guarantees that $Y_u \neq Y_d$. We also discuss how this framework can be extended to yield realistic masses and mixings for the charged leptons and neutrinos.

Our paper is organized as follows. In Section 2, we introduce the general setup of our PS flavour theory and discuss the various scales of symmetry breaking. Moreover, we deduce approximate expressions for the Yukawa matrices as well as the effective light neutrino mass matrix. Section 3 focuses on the flavour structure of the quark sector. We derive analytic formulas for the transformations from the flavour to the mass basis in order to extract the (non-standard) couplings of the quarks to the SM gauge bosons and the Higgs. In Section 4, we describe the method we have used to scan over the parameter space of the model. The results of this numerical scan are presented and discussed in detail in Section 5. We conclude in Section 6. Supplementary material and more technical details are provided in the Appendix.

2 Pati-Salam model with gauged flavour symmetry

As outlined in the introduction, our starting point is a non-supersymmetric high-energy theory with an underlying Pati-Salam gauge symmetry. A manifest left-right symmetric setup is realized by enforcing a discrete Z_2 symmetry. The flavour symmetry group in PS is defined by the independent transformations of the two fermion representations which are used to embed the SM fermions. In the following, we restrict ourselves to the flavour group $SU(3)_I \times SU(3)_{II}$, where the left-chiral SM fermions transform as triplets under $SU(3)_I$ while the right-chiral SM fermions furnish triplet representations of $SU(3)_{II}$. This flavour symmetry, which we assume to be gauged, is spontaneously broken by the VEVs of flavon fields. By the usual Higgs mechanism, the associated Goldstone modes will become the longitudinal degrees of freedom of sixteen new heavy gauge bosons of the

flavour group.² Notice that the maximal flavour-symmetry group in PS is smaller than in the SM, where we encounter a $U(3)^3$ symmetry in the quark sector (as discussed in the original GRV paper [39]) and a $U(3)^2$ symmetry in the lepton sector. To summarize, the full symmetry of the Lagrangian is given by

$$\mathcal{G} = \underbrace{\left(SU(4) \times SU(2) \times SU(2)' \right)}_{\text{Pati-Salam}} \times \underbrace{\left(SU(3)_I \times SU(3)_{II} \right)}_{\text{flavour}} \times Z_2, \quad (2.1)$$

where the global Z_2 symmetry is realized such that a general representation Ω of \mathcal{G} is transformed into $\tilde{\Omega}$ of \mathcal{G} as

$$\Omega = (\omega_c, \omega, \omega')(\omega_I, \omega_{II}) \xrightarrow{Z_2} \tilde{\Omega} = (\bar{\omega}_c, \omega', \omega)(\bar{\omega}_{II}, \bar{\omega}_I). \quad (2.2)$$

Here and in the following, ω denotes a representation of the corresponding group factor and $\bar{\omega}$ is its complex conjugate. As we will only introduce (pseudo-)real representations of $SU(2) \times SU(2)'$, we have dropped the complex conjugation of the corresponding representations in $\tilde{\Omega}$ on the right-hand side of Eq. (2.2).

2.1 Particle content and renormalizable Lagrangian

The left- and right-chiral SM fermions q_L and q_R (including the right-chiral neutrino) are embedded in the $(\mathbf{4}, \mathbf{2}, \mathbf{1})(\mathbf{3}, \mathbf{1})$ and $(\mathbf{4}, \mathbf{1}, \mathbf{2})(\mathbf{1}, \mathbf{3})$ representations of \mathcal{G} . Notice that the transformation of Eq. (2.2) maps the right-chiral fermions q_R into the complex conjugate \bar{q}_L of the left-chiral fermions. Therefore, the chirality of the spinors remains unchanged under a Z_2 transformation. The SM Higgs is embedded in the bi-doublet $H \sim (\mathbf{1}, \mathbf{2}, \mathbf{2})(\mathbf{1}, \mathbf{1})$, which effectively generates the structure of a two-Higgs-doublet model. In order to generalize the idea of GRV, it is necessary to introduce a set of new fermions, denoted as $\Sigma_{L,R}$, $\Xi_{L,R}$. The former, i.e. Σ_L and Σ_R , transform as $(\mathbf{4}, \mathbf{1}, \mathbf{2})(\mathbf{1}, \mathbf{3})$ and $(\mathbf{4}, \mathbf{1}, \mathbf{2})(\mathbf{3}, \mathbf{1})$, while the complex conjugate of the latter, i.e. $\bar{\Xi}_{L,R}$, correspond to the Z_2 conjugated representations of $\Sigma_{R,L}$. Since we impose an exact Z_2 symmetry, we have to introduce both pairs.

Due to the single Higgs bi-doublet H , a flavour symmetry breaking flavon field S transforming trivially under PS cannot discriminate between the up-type and the down-type sector. In contrast to the original GRV model [39], it is therefore impossible to generate a non-trivial flavour structure without mediating the $SU(2)'$ breaking of the PS sector to the flavour sector. As a consequence, we are led to introduce PS non-singlet flavon fields, where the simplest case is realized by $T \sim (\mathbf{1}, \mathbf{3}, \mathbf{1})(\bar{\mathbf{3}}, \mathbf{3})$ and $T' \sim (\mathbf{1}, \mathbf{1}, \mathbf{3})(\bar{\mathbf{3}}, \mathbf{3})$, in addition to the singlet flavon S .

The particle content defined up to this point treats quarks and leptons on equal footing. In particular, neutrinos would be Dirac particles which copy the hierarchical pattern of the up-type quarks. In order to account for the evident difference of quark and lepton flavour, we take advantage of the possibility to generate Majorana mass terms for

²The Yukawa sector is additionally invariant under three independent $U(1)$ symmetries: two associated with $SU(3)_I \times SU(3)_{II}$, while the third relates to the neutrino extension of the theory. All three are broken spontaneously by flavons of the neutrino sector. Massless Goldstone modes can, however, be avoided by breaking the $U(1)$ symmetries explicitly in the scalar potential, for instance by terms involving the determinant of flavon fields.

	Pati-Salam Symmetry $SU(4) \times SU(2) \times SU(2)'$	Flavour Symmetry $SU(3)_I \times SU(3)_{II}$	VEV
\bar{q}_L	$(\bar{4}, 2, 1)$	$(\bar{3}, 1)$	—
q_R	$(4, 1, 2)$	$(1, 3)$	—
H	$(1, 2, 2)$	$(1, 1)$	v_u, v_d
$\bar{\Sigma}_L$	$(\bar{4}, 1, 2)$	$(1, \bar{3})$	—
Σ_R	$(4, 1, 2)$	$(3, 1)$	—
$\bar{\Xi}_L$	$(\bar{4}, 2, 1)$	$(1, \bar{3})$	—
Ξ_R	$(4, 2, 1)$	$(3, 1)$	—
T	$(1, 3, 1)$	$(\bar{3}, 3)$	0
T'	$(1, 1, 3)$	$(\bar{3}, 3)$	$\pm t' M$
S	$(1, 1, 1)$	$(\bar{3}, 3)$	$s M$
$\bar{\Theta}_L$	$(1, 1, 1)$	$(\bar{3}, 8)$	—
Θ_R	$(1, 1, 1)$	$(8, 3)$	—
S_ν	$(1, 1, 1)$	$(6, 1)$	$s_\nu \Lambda_\nu$
S'_ν	$(1, 1, 1)$	$(1, \bar{6})$	$s'_\nu \Lambda_\nu$
Φ	$(4, 2, 1)$	$(8, 1)$	0
Φ'	$(\bar{4}, 1, 2)$	$(1, 8)$	$\varphi' \Lambda_\varphi$

Table 1: The particle content of the theory with imposed Pati-Salam and flavour symmetry. Left- and right-chiral fermions $\psi_{L,R}$ are denoted by subscripts L and R , respectively. The VEVs of the scalar fields (no subscript L or R) are given in the rightmost column. The lower part of the table shows fields necessary for generating Majorana neutrino masses.

electrically neutral leptons. Demanding renormalizability, it is necessary to extend the particle content by further fermionic and scalar fields. Although not unique, there exists a preferred extension (see Appendix A.1) in which additional PS-neutral fermions $\bar{\Theta}_L$ and Θ_R acquire Majorana masses via their coupling to new flavour symmetry breaking flavons S_ν and S'_ν . Furthermore, $\bar{\Theta}_L$ and Σ_R (Θ_R and $\bar{\Xi}_L$) are coupled to one another by means of yet another flavon field Φ' (Φ). Transforming as $(\bar{4}, 1, 2)$ under PS, the vacuum expectation value of the flavon Φ' breaks the Pati-Salam gauge symmetry in the direction of the SM singlet, thereby projecting out the SM neutral component of Σ_R . This in turn couples to the neutrino component of \bar{q}_L (either directly or indirectly via $\bar{\Sigma}_L$ and q_R) which eventually generates a Majorana mass for the left-chiral neutrino \bar{q}_L^ν .

The particle content of the model required for the description of quark and lepton masses and mixing is summarized in Table 1, together with the corresponding transformation properties under the underlying PS and flavour symmetry. Note that we list all fermions using only right-chiral degrees of freedom, i.e. ψ_R and the Dirac adjoint $\bar{\psi}_L$ (instead of ψ_L). As each particle is accompanied by its Z_2 conjugate partner, the PS anomaly $[SU(4)]^3$ vanishes by construction. Concerning the flavour anomalies $[SU(3)_I]^3$ and $[SU(3)_{II}]^3$, it is straightforward to check that the number of fermionic triplets matches the number of fermionic anti-triplets. Notice that we have chosen the octet representa-

tion in $\bar{\Theta}_L$ and Θ_R in order to reflect the dimension of the PS representation of the other fermions. As the adjoint does not contribute to the $SU(3)$ anomaly, both flavour anomalies vanish identically. Mixed anomalies do not exist due to the absence of $U(1)$ factors in \mathcal{G} of Eq. (2.1). Hence the model presented in Table 1 is free of any gauge anomaly.

With the particle content specified in Table 1, it is straightforward to formulate the most general renormalizable Yukawa Lagrangian which is invariant under the full symmetry \mathcal{G} . Collecting all terms which involve the heavy fermions $\Theta_{L,R}$ (required to generate light Majorana neutrino masses) in $\mathcal{L}_{\text{Yuk}}^\nu$, we can write

$$\mathcal{L}_{\text{Yuk}} = \mathcal{L}_{\text{Yuk}}^q + \mathcal{L}_{\text{Yuk}}^\nu, \quad (2.3)$$

where

$$\begin{aligned} \mathcal{L}_{\text{Yuk}}^q = & \lambda \bar{q}_L H \Sigma_R + \bar{\Sigma}_L (\kappa_S S + \kappa_T T') \Sigma_R + M \bar{\Sigma}_L q_R + h.c. \\ & + \lambda \bar{\Xi}_L H q_R + \bar{\Xi}_L (\kappa_S S + \kappa_T T) \Xi_R + M \bar{q}_L \Xi_R + h.c., \end{aligned} \quad (2.4)$$

and

$$\begin{aligned} \mathcal{L}_{\text{Yuk}}^\nu \sim & \bar{\Theta}_L \Phi' \Sigma_R + \frac{1}{2} \bar{\Theta}_L S_\nu \bar{\Theta}_L + h.c. \\ & + \bar{\Xi}_L \Phi \Theta_R + \frac{1}{2} \Theta_R S'_\nu \Theta_R + h.c. \\ & + \bar{\Theta}_L S^\dagger \Theta_R + h.c. . \end{aligned} \quad (2.5)$$

In Eqs. (2.4) and (2.5), the terms of the first line are related to those of the second line through the action of the Z_2 symmetry. The term in the third line of Eq. (2.5) is its own Z_2 conjugate. Due to these relations, the Yukawa Lagrangian $\mathcal{L}_{\text{Yuk}}^q$ depends on only four independent parameters: three dimensionless couplings λ , κ_S , κ_T , and one mass scale M . Redefining the phases of the fermions, it is clear that λ and M can be chosen real and positive without loss of generality. As κ_S and κ_T appear only in combination with the flavon fields which will generally acquire complex VEVs, their phases can be kept arbitrary at this point. With regard to the neutrino Lagrangian $\mathcal{L}_{\text{Yuk}}^\nu$, we are at this point only interested in a qualitative analysis. Therefore, we have suppressed explicit coupling constants, which would again be related by the Z_2 symmetry, in Eq. (2.5).

2.2 Symmetry breaking and mass scales

The flavour structure of the SM fermions originates in the flavon fields. Assigning VEVs of order M or higher for the components of S and T' , breaks the flavour symmetry $SU(3)_I \times SU(3)_{II}$ above the electroweak scale v . The scalar field T , on the other hand, must not get a high scale VEV as it transforms as an $SU(2)$ triplet. However, a possible mixing with the electroweak Higgs doublets would generically induce a VEV $\langle T \rangle$ below the electroweak scale at order v^2/M . As the impact of this VEV on the flavour structure is negligible compared to $\langle S \rangle$, we will approximate $\langle T \rangle \simeq 0$ in the following, for simplicity. In order to obtain a phenomenologically realistic difference between the effective Yukawa matrices of the up and the down quarks, we need the singular values of the VEVs $\langle S \rangle$ and $\langle T' \rangle$ to be of similar size.

In addition to breaking the flavour symmetry, the VEV $\langle T' \rangle$ breaks $SU(2)'$ as well. In order to keep the standard charge assignments for up- and down-type quarks, we choose $\langle T' \rangle$ to be aligned along the τ_3 direction of $SU(2)'$. Its smallest singular value is considered to be (at least) of the order of the scale M . Factoring out this explicit mass scale, we parameterize the vacuum structure responsible for the Yukawa matrices of the charged fermions as follows,

$$\kappa_S \langle S \rangle = s M \quad \text{and} \quad \kappa_T \langle T' \rangle = \begin{pmatrix} t' & 0 \\ 0 & -t' \end{pmatrix} M, \quad (2.6)$$

where s and t' are defined as dimensionless 3×3 matrices in flavour space.

Turning to the neutrino sector, we adopt the double seesaw mechanism [58] involving \bar{q}_L , Σ_R and $\bar{\Theta}_L$.³ The PS-neutral fermions $\bar{\Theta}_L$ acquire a Majorana mass $\langle S_\nu \rangle$ at a high scale Λ_ν . Furthermore, a Dirac mass term $\bar{\Theta}_L \langle \Phi' \rangle \Sigma_R$ is generated at the scale $\Lambda_\varphi \ll \Lambda_\nu$. With this hierarchy of scales, the first stage of the double seesaw mechanism gives rise to a Majorana neutrino mass for the SM neutral component Σ_R^ν within Σ_R . In the second stage of the double seesaw, light Majorana neutrino masses for the left-chiral neutrinos \bar{q}_L^ν are induced via the Dirac coupling of \bar{q}_L^ν and Σ_R^ν . Analogous to Eq. (2.6), we parameterize the VEVs of the scalar fields required for generating light Majorana neutrino masses as

$$\langle S_\nu \rangle = s_\nu \Lambda_\nu, \quad \langle S'_\nu \rangle = s'_\nu \Lambda_\nu, \quad \text{and} \quad \langle \Phi' \rangle = \varphi' \Lambda_\varphi. \quad (2.7)$$

Here we have included the VEV of S'_ν which will turn out to be crucial for the construction of the lepton sector as discussed in Appendix A.1. The quantities s_ν , s'_ν and φ' are again dimensionless tensor structures in flavour space. Note that Φ transforms non-trivially under the electroweak symmetry. Similar to T , it must therefore not receive a high scale VEV, and we will approximate $\langle \Phi \rangle \simeq 0$ in the following.

In contrast to the original GRV model proposed in [39], in our setup the flavour gauge bosons do not play an essential role for the low-energy phenomenology. The reason for this is the inclusion of the lepton/neutrino sector which requires the introduction of the flavons S_ν , S'_ν and Φ' in addition to S and T' . While the latter acquire VEVs reaching down to the scale M (TeV regime), the former obtain their VEVs at much larger scales, Λ_ν and Λ_φ . As these are related to the type I seesaw scale via $\Lambda_\varphi^2/\Lambda_\nu \sim M_{\text{seesaw}}$, it is reasonable to assume a typical hierarchy of scales,

$$10^{10} \text{ GeV} \lesssim \Lambda_\varphi \ll \Lambda_\nu \lesssim M_{\text{Planck}} \sim 10^{18} \text{ GeV}. \quad (2.8)$$

Here, the lower bound is relatively flexible (due to the vague definition of M_{seesaw}) and has been chosen rather conservatively. As a consequence, the gauged flavour symmetry gets broken at a very large scale, and the associated flavour gauge bosons become too heavy to be relevant for current or future particle physics experiments. In principle, a subset of the flavour gauge bosons could remain massless down to lower scales. However, if the symmetric 3×3 matrix s_ν has non-vanishing and non-degenerate singular values,

³There exists another contribution to the effective light neutrino masses which additionally involves the fields $\bar{\Sigma}_L$, q_R , $\bar{\Xi}_L$ and Ξ_R . Its structure will automatically become manifest when integrating out the heavy degrees of freedom in \mathcal{L}_{Yuk} .

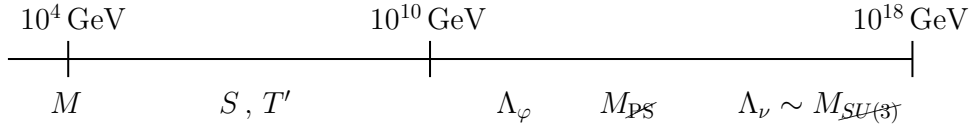


Figure 1: Illustration of the hierarchy of scales introduced in the PS model with gauged flavour symmetry. The numerical values are shown as an indicative example only. $M_{SU(3)}$ denotes the scale of the flavour gauge bosons, while M_{PS} is the scale of the heavy PS gauge bosons.

$SU(3)_I$ gets fully broken and all its flavour gauge bosons acquire masses at the scale Λ_ν . Similarly, all flavour gauge bosons of $SU(3)_{II}$ become heavy due to $\langle S'_\nu \rangle$.

Concerning the masses of the gauge bosons associated with the PS symmetry, we point out that we do not fully specify the breaking of $SU(4)$ or $SU(2)'$. Yet, already the flavon Φ' , which we have introduced for the purpose of generating light neutrino masses, breaks PS down to the SM [10, 59]. Therefore, the masses of the non-SM gauge bosons, including the W'^{\pm} and the Z' , are bounded from below by Λ_φ . Additional PS breaking fields may lead to even larger masses.

As discussed above, the various scales of the model are only partially constrained. Their ordering is, however, determined as illustrated in Fig. 1. In addition to the hierarchies of scales, the singular values of $\langle S \rangle$ and $\langle T' \rangle$ feature internal hierarchies, with the smallest reaching down to the scale M . The value of M is bounded from below by flavour precision observables as well as the non-observation of new charged fermionic states. For the purpose of our numerical parameter scan, we will assume values of a few TeV. Due to the strong hierarchy of quark masses, the largest singular values of $\langle S \rangle$ and $\langle T' \rangle$ take numerical values up to order 10^{10} GeV. This is in fact the reason for choosing the lower bound on Λ_φ as given in Eq. (2.8). On the other hand, Λ_φ is bounded from above by the GUT scale M_{GUT} , as $\langle \Phi' \rangle$ breaks PS down to the SM. Finally, the largest scale Λ_ν must lie between Λ_φ and the Planck scale M_{Planck} . In addition to these scales, Fig. 1 also shows the mass scale $M_{SU(3)}$ of the flavour gauge bosons as well as the mass scale M_{PS} of the heavy PS gauge bosons as discussed above.

Strictly speaking, the model is formulated at the GUT scale. Due to the presence of multiple scales, it is generally necessary to consider threshold corrections at each of these scales. In what follows, we will, however, neglect such effects as we do not aim for a comprehensive top-down description of the model. We will therefore perform our numerical scan using flavour parameters (e.g. quark masses) which are fixed at the Z boson mass scale.

2.3 Approximate flavour structure of quarks and leptons

In a first step to understand the structure of the low-energy effective Lagrangian derived from Eq. (2.3), we formally integrate out the heavy degrees of freedom. The result will provide reasonably simple expressions for the approximate flavour structure of quarks and leptons. We begin our discussion with the quark sector, where all relevant terms are included in $\mathcal{L}_{\text{Yuk}}^q$ of Eq. (2.4). Assuming for the moment all VEVs of S and T' to be significantly larger than the intrinsic mass scale M , i.e. $s \sim t' \gg 1$, we can integrate out

the heavy fermions $\Sigma_{L,R}$ and $\Xi_{L,R}$.⁴ Defining the 3×3 matrices

$$t_u \equiv s + t' , \quad t_d \equiv s - t' , \quad (2.9)$$

the resulting effective Yukawa potential takes the form

$$\begin{aligned} \mathcal{L}_{\text{Yuk}}^{q,\text{eff}} = & -\lambda h_u^0 \bar{q}_L^u [t_u^{-1} + s^{-1}] q_R^u + h.c. \\ & -\lambda h_d^0 \bar{q}_L^d [t_d^{-1} + s^{-1}] q_R^d + h.c. , \end{aligned} \quad (2.10)$$

where the $SU(2)$ and $SU(2)'$ doublets have been explicitly decomposed into their up and down components. The effective couplings correspond to the standard quark Yukawa matrices in a two-Higgs-doublet model, and can be directly read off as

$$Y_{u,d} \simeq -\lambda [t_{u,d}^{-1} + s^{-1}] . \quad (2.11)$$

It is worth mentioning that this relation between the flavon VEVs and the SM Yukawa matrices is neither a linear one as in Minimal-Flavour Violation (MFV) [60–64] nor a simple inverse one as in [39], where the difference with the latter can be traced back to the imposed Z_2 symmetry. Yet, similarly to the original GRV case, the expressions in Eq. (2.11) show that the observed hierarchy of the Yukawa matrices is turned into an inverse hierarchy of the 3×3 matrices s and t' . Eq. (2.11) can now be used to fit the 19 independent parameters of s and t' (six singular values, six mixing angles and seven phases) to the quark masses and the CKM matrix V_{CKM} . In contrast to the SM, the mixing of the right-chiral quarks (parameterized by U'_{CKM} in the following) is physical in our PS model and has to be kept as a consequence. As the relation between $Y_{u,d}$ and s, t' is given by a coupled matrix equation, it is a non-trivial task to invert Eq. (2.11). We describe the method used to obtain numerical results for s and t' in Appendix B.

An important feature, already arising at this stage, is the existence of multiple solutions when inverting Eq. (2.11). This can be easily understood in the case of one generation, where the resulting two solutions can be expressed analytically. Explicitly, we find

$$s = \frac{-8\lambda}{3y_u + 3y_d \mp 3\sqrt{(y_u - y_d)^2 + \frac{4}{9}y_u y_d}} , \quad (2.12a)$$

$$t_u = \frac{-8\lambda}{5y_u - 3y_d \pm 3\sqrt{(y_u - y_d)^2 + \frac{4}{9}y_u y_d}} , \quad (2.12b)$$

with $y_{u,d}$ denoting the one-generation up-type and down-type Yukawa couplings. Using these expressions it is straightforward to determine t' as well as t_d . Extending this result to three generations gives rise to a total of eight solutions for s and t' . We emphasize that all of these generate the same approximate Yukawa matrices via Eq. (2.11). However, as we will see in Section 5, different solutions may generate different phenomenological predictions beyond the SM.

⁴To be precise, considering the quark sector, we only have to integrate out the colour (anti-)triplets contained in the (anti-)fundamental representations of $SU(4)$.

Turning to the lepton sector, we first remark that the structure of the charged lepton Yukawa matrix is identical to the one of the down-type quarks. This is a common feature to the simplest Pati-Salam models and a reasonably good first approximation. Possible modifications to the charged lepton sector are briefly sketched in Appendix A.2. In the neutrino sector, the Lagrangian involving the heavy fermions $\Theta_{L,R}$ generates a Majorana mass term for the neutrino component Σ_R^ν within the PS multiplet Σ_R . Integrating out $\Theta_{L,R}$ in $\mathcal{L}_{\text{Yuk}}^\nu$ of Eq. (2.5) yields

$$\mathcal{L}_{\text{Yuk}}^{\nu,\text{eff}} \sim - \frac{(\varphi'_\alpha \Lambda_\varphi)^2}{2 \Lambda_\nu} \Sigma_R^\nu s_\nu^{-1} \Sigma_R^\nu. \quad (2.13)$$

We remark that s_ν is a symmetric 3×3 matrix in $SU(3)_I$ flavour space, while $\varphi'_\alpha \Lambda_\varphi$ denotes the VEV of Φ' which points in the direction of the SM neutral component of the PS representation $(\bar{4}, \mathbf{1}, \mathbf{2})$. Being an octet of $SU(3)_{II}$, φ'_α with $\alpha = 1, \dots, 8$ does not affect the flavour structure of the neutrino sector. Combining this Majorana mass term for Σ_R^ν with the couplings of the electromagnetically neutral fermions in $\mathcal{L}_{\text{Yuk}}^q$ of Eq. (2.4) generates Majorana masses for the left-chiral neutrinos. The resulting structure of the neutrino mass matrix can be obtained by formally integrating out the heavy neutral fermions Σ_R^ν and $\Xi_{L,R}^\nu$ as well as Σ_L^ν and q_R^ν . It is given by

$$m_\nu^{\text{eff}} \sim \frac{\Lambda_\nu v_u^2}{2 (\varphi'_\alpha \Lambda_\varphi)^2} (\mathbb{1} + s^{-1} t_u) s_\nu (\mathbb{1} + s^{-1} t_u)^T, \quad (2.14)$$

where $v_u/\sqrt{2}$ denotes the VEV of the neutral Higgs h_u^0 , cf. Appendix A.1. It is important to note that the flavour structure of the light neutrinos is decoupled from the quark sector. In particular, the distinct hierarchical structure of s and t_u is approximately cancelled in the combination $s^{-1} t_u$, such that the structure of the effective neutrino mass matrix is mainly determined by s_ν . As a consequence, the PMNS mixing of the lepton sector can be significantly different from the CKM mixing of the quarks. Assuming the dimensionless parameters $s^{-1} t_u$, s_ν and φ'_α to be of order one, we find that $\Lambda_\varphi \sim 10^{16} \text{GeV} \sim M_{\text{GUT}}$ and $\Lambda_\nu \sim 10^{18} \text{GeV} \sim M_{\text{Planck}}$ gives rise to realistic neutrino masses of the order 0.1 eV. As such, the model provides sufficient freedom to construct a phenomenologically viable lepton sector. More detailed studies are left for future work.

3 Quark flavour sector

The effective quark flavour structure derived in Section 2.3 is only an approximation which relies on the simplifying assumption that $s, t' \gg 1$. Clearly, such a relation is not satisfied for the Yukawa couplings of the third generation of quarks which should be of order one for the top quark (and, depending on $\tan \beta = v_u/v_d$, also for the bottom quark). Taking this fact into account, it is necessary to diagonalize the full 9×9 mass matrices of the SM quarks and their heavy partners. The corresponding transformations are then applied to the gauge-kinetic sector in order to extract the characteristic features of the effective low-energy quark flavour sector. We also comment on the coupling of the Higgs field to the SM quarks, which is no longer fully aligned with the diagonal quark mass matrices.

3.1 Diagonalizing the quark mass matrices

In this subsection, we re-examine the Yukawa Lagrangian of Eq. (2.4). Assigning VEVs to the flavour symmetry breaking fields S and T' as well as the $SU(2) \times SU(2)'$ bi-doublet H , Eq. (2.4) gives rise to

$$\mathcal{L}_{\text{mass}}^q = \frac{1}{\sqrt{2}} \lambda v_u \bar{q}_L^u \Sigma_R^u + M \bar{\Sigma}_L^u t_u \Sigma_R^u + M \bar{\Sigma}_L^u q_R^u + h.c. \quad (3.1a)$$

$$+ \frac{1}{\sqrt{2}} \lambda v_u \bar{\Xi}_L^u q_R^u + M \bar{\Xi}_L^u s \Xi_R^u + M \bar{q}_L^u \Xi_R^u + h.c. \quad (3.1b)$$

$$+ (u \leftrightarrow d) .$$

Collecting the left-chiral (right-chiral) fermions in Ψ_L (Ψ_R), these bilinear mass terms can be compactly written as $\bar{\Psi}_L^u \mathcal{M}^u \Psi_R^u$ and $\bar{\Psi}_L^d \mathcal{M}^d \Psi_R^d$. For definiteness, we focus on the up-type quark sector in the rest of this subsection. Analogous results arise for the down-type quark sector, and the corresponding expressions are obtained by simply replacing the index u by d . Defining

$$\bar{\Psi}_L^u \equiv (\bar{q}_L^u, \bar{\Sigma}_L^u, \bar{\Xi}_L^u) , \quad \Psi_R^u \equiv (q_R^u, \Sigma_R^u, \Xi_R^u) , \quad (3.2)$$

the 9×9 mass matrix takes the form

$$\mathcal{M}^u = \begin{pmatrix} 0 & \mathbb{1} \lambda \epsilon_u & \mathbb{1} \\ \mathbb{1} & t_u & 0 \\ \mathbb{1} \lambda \epsilon_u & 0 & s \end{pmatrix} M , \quad (3.3)$$

where each entry corresponds itself to a 3×3 matrix in generation space. The quantity

$$\epsilon_u \equiv \frac{v_u}{\sqrt{2} M} \ll 1 \quad (3.4)$$

can be treated as a small expansion parameter. In the following, we describe the sequence of basis transformations which diagonalizes \mathcal{M}^u of Eq. (3.3) in powers of ϵ_u up to quadratic order. More technical details of this diagonalization are relegated to Appendix C.

In the first step, we make use of the $SU(3)_I \times SU(3)_{II}$ flavour symmetry to diagonalize the 3×3 matrix s in Eq. (3.3). This corresponds to a choice of basis which can always be made without loss of generality. We can thus simply replace s by \hat{s} , where here and in the following the hat denotes a diagonal matrix. Next, we apply a bi-unitary basis transformation to diagonalize the submatrix t_u , i.e.

$$\hat{t}_u = V_u t_u U_u^\dagger . \quad (3.5)$$

Having exhausted the flavour symmetry by choosing a diagonal \hat{s} , the unitary 3×3 matrices V_u and U_u will reappear elsewhere in the full mass matrix. As discussed in Appendix C, they can however be shifted to the ϵ_u -suppressed blocks. In the limiting case of $\epsilon_u = 0$, the resulting mass matrix takes the form of Eq. (3.3) with s and t_u replaced by \hat{s} and \hat{t}_u . In this limit, the three generations decouple from one another and the 9×9 matrix decomposes into three 3×3 blocks, one for each generation i . Introducing only two mixing angles for each generation (whose values depend on \hat{s} and \hat{t}_u), it is

straightforward to diagonalize these blocks exactly. In the third step, we therefore apply such a transformation to the full mass matrix including the ϵ_u -suppressed blocks. This gives rise to a mass matrix of the form

$$\mathcal{M}^u \rightarrow \begin{pmatrix} a_u \epsilon_u & b_u \epsilon_u & 0 \\ 0 & \hat{e}_u & 0 \\ c_u \epsilon_u & d_u \epsilon_u & \hat{f} \end{pmatrix} M, \quad (3.6)$$

where the 3×3 matrices a_u , b_u , c_u , d_u , \hat{e}_u and \hat{f} depend on V_u , U_u as well as the above mentioned mixing. The explicit expressions are given in Appendix C. Note that the mass matrix in Eq. (3.6) is diagonal at zeroth order in the expansion parameter. Block-diagonalization to second order in ϵ_u requires an intricate basis transformation which can be found in Appendix C. Yet, the resulting mass matrix simply reads

$$\mathcal{M}^u \rightarrow \begin{pmatrix} a_u \epsilon_u & 0 & 0 \\ 0 & \hat{e}_u + \mathcal{O}(\epsilon_u^2) & 0 \\ 0 & 0 & \hat{f} + \mathcal{O}(\epsilon_u^2) \end{pmatrix} M + \mathcal{O}(\epsilon_u^3) M. \quad (3.7)$$

The remaining transformation needed to render this matrix completely diagonal (up to order ϵ_u^2) involves only rotations within the three non-vanishing 3×3 blocks. These do not mix the light quarks with the heavy partners. Due to our lack of experimental data on any heavy fermions, it is safe to ignore the corresponding 3×3 rotations which would take the general form $\mathbb{1} + \mathcal{O}(\epsilon_u^2)$. For the three light quarks on the other hand, we define the bi-unitary transformation which diagonalizes a_u ,

$$\hat{Y}_u = \mathcal{V}_u a_u \mathcal{U}_u^\dagger. \quad (3.8)$$

The complete sequence of transformations diagonalizes the 9×9 quark mass matrix of Eq. (3.3) up to second order in ϵ_u . It therefore constitutes the change from the original flavour basis $\Psi_{L,R}^{u,d}$ to the approximate mass basis $\Psi_{L,R}'^{u,d}$. The individual steps of this change of basis are explicitly given in Appendix C. In the next subsection, we will apply these transformations to the gauge-kinetic sector.

3.2 Gauge-kinetic terms

As discussed in Section 2.2, the flavour gauge bosons are far beyond the reach of current or future particle physics experiments. They are therefore phenomenologically irrelevant and we do not consider them any further. Concerning the 15 gauge bosons associated with the $SU(4)$ factor of the PS symmetry we note that 6 become extremely massive and irrelevant when $SU(4) \rightarrow SU(3)_c \times U(1)_{B-L}$. Moreover, the 8 gluons of $SU(3)_c$ are flavour blind and can be ignored as well. The remaining $U(1)_{B-L}$ boson will mix with the neutral gauge bosons of $SU(2) \times SU(2)'$ and has to be kept. Being mainly interested in the flavour structure, it is therefore sufficient to focus on the gauge-kinetic terms corresponding to the $SU(2) \times SU(2)' \times U(1)_{B-L}$ part of the PS symmetry. In order to be able to apply the sequence of basis transformations described above (and in Appendix C), we express the relevant gauge-kinetic terms by means of the left- and right-chiral vectors Ψ_L and Ψ_R

defined in Eq. (3.2). In this context, it is important to realize that Ψ_L does not solely contain doublets of $SU(2)$ but also doublets of $SU(2)'$. Likewise, Ψ_R contains doublets of both $SU(2)'$ and $SU(2)$. Taking this fact into account, the relevant gauge-kinetic terms read

$$\begin{aligned}\mathcal{L}_{\text{kin}} \supset & \bar{\Psi}_L \left(g \vec{W} \vec{\tau} \right) \mathcal{K}_L \Psi_L + \bar{\Psi}_R \left(g \vec{W} \vec{\tau} \right) \mathcal{K}_R \Psi_R \\ & + \bar{\Psi}_L \left(g \vec{W}' \vec{\tau} \right) \mathcal{K}'_L \Psi_L + \bar{\Psi}_R \left(g \vec{W}' \vec{\tau} \right) \mathcal{K}'_R \Psi_R \\ & + \bar{\Psi}_L \left(\frac{1}{2} g_{B-L} Q_{B-L} \vec{B}_{B-L} \right) \Psi_L + \bar{\Psi}_R \left(\frac{1}{2} g_{B-L} Q_{B-L} \vec{B}_{B-L} \right) \Psi_R ,\end{aligned}\quad (3.9)$$

where Q_{B-L} is the difference of baryon and lepton number, and the \mathcal{K} matrices

$$\mathcal{K}_L = \begin{pmatrix} \mathbb{1} & 0 & 0 \\ 0 & 0 & 0 \\ 0 & 0 & \mathbb{1} \end{pmatrix} , \quad \mathcal{K}_R = \begin{pmatrix} 0 & 0 & 0 \\ 0 & 0 & 0 \\ 0 & 0 & \mathbb{1} \end{pmatrix} , \quad (3.10a)$$

$$\mathcal{K}'_L = \begin{pmatrix} 0 & 0 & 0 \\ 0 & \mathbb{1} & 0 \\ 0 & 0 & 0 \end{pmatrix} , \quad \mathcal{K}'_R = \begin{pmatrix} \mathbb{1} & 0 & 0 \\ 0 & \mathbb{1} & 0 \\ 0 & 0 & 0 \end{pmatrix} , \quad (3.10b)$$

encode the non-trivial $SU(2) \times SU(2)'$ transformation properties of Ψ_L and Ψ_R . Here we emphasize that the $SU(2)$ gauge bosons couple to both left- and right-chiral fermions. Likewise, the $SU(2)'$ gauge bosons couple to fermions of both chiralities.

While breaking $SU(2)' \times U(1)_{B-L} \rightarrow U(1)_Y$ the neutral bosons $W'^{(3)}$ and B_{B-L} mix, resulting in a massless B_Y and a massive Z' boson. Analogous to the electroweak symmetry breaking in the SM, this mixing is described by s'_W and c'_W which satisfy $g s'_W = g_{B-L} c'_W \equiv g_Y$. The charged $SU(2)'$ gauge bosons $W'^{\pm} \equiv (W'^1 \mp i W'^2)/\sqrt{2}$ become massive from the $SU(2)'$ breaking as well. As this breaking arises at an extremely high scale, cf. Figure 1, the W'^{\pm} and Z' gauge bosons are irrelevant for low-energy flavour effects. In a second step, the breaking $SU(2) \times U(1)_Y \rightarrow U(1)_{\text{em}}$ at the electroweak scale induces a mixing of the neutral gauge bosons W^3 and B_Y which is parameterized by s_W and c_W satisfying $g s_W = g_Y c_W \equiv e$. Using these relations and the two-step mixing

$$\vec{B}_{B-L} = c'_W (c_W \vec{A} - s_W \vec{Z}) - s'_W \vec{Z}' , \quad (3.11a)$$

$$\vec{W}'^3 = s'_W (c_W \vec{A} - s_W \vec{Z}) + c'_W \vec{Z}' , \quad (3.11b)$$

$$\vec{W}^3 = s_W \vec{A} + c_W \vec{Z} , \quad (3.11c)$$

we can rewrite the gauge-kinetic Lagrangian, keeping only the terms which are relevant for low-energy flavour effects,

$$\begin{aligned}\mathcal{L}_{\text{kin}} \supset & \bar{\Psi}_L \frac{g}{\sqrt{2}} \mathcal{K}_L (\tau^1 \pm i \tau^2) W^{\pm} \Psi_L \\ & + \bar{\Psi}_L \frac{g}{c_W} \left((c_W^2 \mathcal{K}_L - s_W^2 \mathcal{K}'_L) \tau^3 - \frac{1}{2} s_W^2 Q_{B-L} \right) Z \Psi_L \\ & + \bar{\Psi}_L e \left((\mathcal{K}_L + \mathcal{K}'_L) \tau^3 + \frac{1}{2} Q_{B-L} \right) A \Psi_L \\ & + (L \leftrightarrow R) .\end{aligned}\quad (3.12)$$

In order to simplify the notation, it is convenient to decompose the isospin doublets in the charged current interactions explicitly into their components. Using the relations $\mathcal{K}_L + \mathcal{K}'_L = \mathcal{K}_R + \mathcal{K}'_R = \mathbb{1}$ as well as⁵ $Q_e = \frac{1}{2} Q_{B-L} + \tau^3$, we obtain

$$\begin{aligned}
\mathcal{L}_{\text{kin}} \supset & \frac{g}{\sqrt{2}} \bar{\Psi}_L^u \mathcal{K}_L W^+ \Psi_L^d + h.c. \\
& + \frac{g}{\sqrt{2}} \bar{\Psi}_R^u \mathcal{K}_R W^+ \Psi_R^d + h.c. \\
& + \frac{g}{c_W} \bar{\Psi}_L \left((\tau^3 - s_W^2 Q_e) \mathbb{1} - \mathcal{K}'_L \tau^3 \right) \not{Z} \Psi_L \\
& + \frac{g}{c_W} \bar{\Psi}_R \left(-s_W^2 Q_e \mathbb{1} + \mathcal{K}_R \tau^3 \right) \not{Z} \Psi_R \\
& + e \left(\bar{\Psi}_L Q_e \not{A} \Psi_L + \bar{\Psi}_R Q_e \not{A} \Psi_R \right). \tag{3.13}
\end{aligned}$$

When applying the sequence of basis transformations discussed above, it is important to take into account the isospin structure of the charged and neutral couplings. As a result, the flavour structure of all terms involving the \mathcal{K} matrices is modified in a non-trivial way, while the form of the remaining terms is left unchanged. For instance, the last line of Eq. (3.13) shows that the coupling of the photon is always diagonal and proportional to the corresponding electric charge. The explicit expressions of the full \mathcal{K} matrices in the approximate mass basis are provided in Appendix C. They will be important when studying the gauge interactions of the light quarks with their heavy partners such as e.g. the coupling $\bar{b} t' W^-$. Being mainly interested in the phenomenological flavour effects involving only the three generations of light quarks $q'_{L,R}$ (where the prime denotes the approximate mass basis), we focus our attention on the upper left 3×3 block. Separating the couplings which are already present in the SM (such as V_{CKM}) from terms which are characteristic to our setup (i.e. ΔV_{CKM} , U_{CKM} , $\Delta g_{Z\bar{q}_L q_L}$ and $\Delta g_{Z\bar{q}_R q_R}$), the terms of the gauge-kinetic Lagrangian take the form

$$\begin{aligned}
\mathcal{L}_{\text{kin}} \supset & \frac{g}{\sqrt{2}} \bar{q}'_L{}^u (V_{\text{CKM}} - \Delta V_{\text{CKM}}) W^+ q'_L{}^d + h.c. \\
& + \frac{g}{\sqrt{2}} \bar{q}'_R{}^u U_{\text{CKM}} W^+ q'_R{}^d + h.c. \\
& + \frac{g}{c_W} \bar{q}'_L \left((\tau^3 - s_W^2 Q_e) \mathbb{1} - \Delta g_{Z\bar{q}_L q_L} \tau^3 \right) \not{Z} q'_L \\
& + \frac{g}{c_W} \bar{q}'_R \left(-s_W^2 Q_e \mathbb{1} + \Delta g_{Z\bar{q}_R q_R} \tau^3 \right) \not{Z} q'_R. \tag{3.14}
\end{aligned}$$

We emphasize that the two matrices $\Delta g_{Z\bar{q}_L q_L}$ and $\Delta g_{Z\bar{q}_R q_R}$ will generally be different for the two isospin components. Mindful of this subtlety, we however suppress the corresponding isospin indices for the sake of notational simplicity. Comparing the explicit expressions of Appendix C, in particular Eq. (C.11), with Eq. (3.14) reveals that the

⁵The relation between the electric charge Q_e and Q_{B-L} takes this simple form as the fermions of the model transform solely under one of the two $SU(2)$ gauge factors. Therefore, τ^3 is understood to act on either $SU(2)$ or $SU(2)'$, depending on the specific particle.



Figure 2: Leading order corrections to the quark masses and the Higgs-quark-quark coupling $g_{h\bar{q}q}$.

low-energy flavour effects are parameterized as follows,

$$V_{\text{CKM}} = \mathcal{V}_u \mathcal{V}_d^\dagger, \quad (3.15a)$$

$$\Delta V_{\text{CKM}} = \frac{1}{2} \mathcal{V}_u \left(b_u \hat{e}_u^{-2} b_u^\dagger \epsilon_u^2 + b_d \hat{e}_d^{-2} b_d^\dagger \epsilon_d^2 \right) \mathcal{V}_d^\dagger + \mathcal{O}(\epsilon_{u,d}^3), \quad (3.15b)$$

$$U_{\text{CKM}} = \mathcal{U}_u c_u^\dagger \hat{f}^{-2} c_d \mathcal{U}_d^\dagger \epsilon_u \epsilon_d + \mathcal{O}(\epsilon_{u,d}^3), \quad (3.15c)$$

$$\Delta g_{Z\bar{q}_L q_L} = \mathcal{V} b \hat{e}^{-2} b^\dagger \mathcal{V}^\dagger \epsilon^2 + \mathcal{O}(\epsilon^3), \quad (3.15d)$$

$$\Delta g_{Z\bar{q}_R q_R} = \mathcal{U} c^\dagger \hat{f}^{-2} c \mathcal{U}^\dagger \epsilon^2 + \mathcal{O}(\epsilon^3). \quad (3.15e)$$

We point out that the effective CKM matrix $V_{\text{CKM}}^{\text{eff}}$ is no longer unitary as it receives a correction ΔV_{CKM} . Like all the other beyond the SM flavour effects, this correction is of second order in the expansion parameters $\epsilon_{u,d}$.

3.3 Non-standard Higgs couplings

As can be seen from the Lagrangian of Eq. (2.4), there exists no direct coupling of the Higgs boson to a pair of SM quarks. Similar to the quark masses, such an interaction is generated effectively through couplings to the heavy quark partners. For this reason, the Higgs-quark-quark coupling $g_{h\bar{q}q}$ is no longer exactly diagonal in generation space nor proportional to the quark masses. The effective expression for $g_{h\bar{q}q}$ can be deduced by formally integrating out the heavy fermions or, alternatively, by explicitly applying the sequence of basis transformations defined above to the Higgs couplings. As a result, we find that the corrections to the quark masses as well as the Higgs-quark-quark coupling are both of order $\epsilon_{u,d}^2$, however, they differ from one another by a combinatorial factor of three.

This effect can be understood by explicitly studying the leading order corrections starting from the basis of Eq. (3.6). We stress that this basis does not make use of any approximation in terms of a truncated $\epsilon_{u,d}$ expansion. Reinserting the original Higgs field in Eq. (3.6), the corresponding diagrams, depicted in Figure 2, lead to an effective coupling of three Higgs bosons to a pair of SM quarks. They provide a correction to the quark masses if all Higgs fields acquire their VEV. Alternatively, if only two of them are set to their VEV, the diagrams of Figure 2 contribute to the Higgs-quark-quark coupling $g_{h\bar{q}q}$. With three possible ways of choosing two Higgs VEVs (and one Higgs field), the latter correction picks up the combinatorial factor of three. Such an effect also occurs in the SM when considering general effective dimension six operators [65].

As the effect arise identically in the up-type as well as the down-type quark sector, we suppress the subscripts u and d in our resulting expression which are valid up to order $\epsilon_{u,d}^2$. In the approximate mass basis, where the three light generations of quarks are denoted by $q'_{L,R}$, the effective Yukawa coupling takes the form

$$Y \approx \hat{Y} - \frac{\epsilon^2}{2} \left[\mathcal{V} b \hat{e}^{-2} b^\dagger \mathcal{V}^\dagger \cdot \hat{Y} + \hat{Y} \cdot \mathcal{U} c^\dagger \hat{f}^{-2} c \mathcal{U}^\dagger \right], \quad (3.16)$$

while the Higgs-quark-quark coupling is given by

$$g_{h\bar{q}q} \approx \hat{Y} - \frac{3\epsilon^2}{2} \left[\mathcal{V} b \hat{e}^{-2} b^\dagger \mathcal{V}^\dagger \cdot \hat{Y} + \hat{Y} \cdot \mathcal{U} c^\dagger \hat{f}^{-2} c \mathcal{U}^\dagger \right]. \quad (3.17)$$

In these expressions, \hat{Y} is the exactly diagonalized version of the matrix a , using the unitary transformations \mathcal{V} and \mathcal{U} , cf. Eq. (3.8). We observe that the Yukawa matrix in Eq. (3.16) is only diagonal up to first order in $\epsilon_{u,d}$. Diagonalizing Y to second (or in fact arbitrary) order can be achieved by small modifications of \mathcal{V} and \mathcal{U} . Applying the same basis transformation to $g_{h\bar{q}q}$ of Eq. (3.17) will generally leave the Higgs-quark-quark coupling non-diagonal at order $\epsilon_{u,d}^2$. Moreover, comparing Eqs. (3.16) and (3.17), it is possible to show that the diagonal couplings of $g_{h\bar{q}q}$ are reduced compared to their SM values. Numerically, we explicitly find such an effect in our scan over model parameters, where we exemplarily show the (normalized) Higgs-top-top coupling in Figure 7(a).

4 Scanning the parameter space

In the previous section, we have calculated analytical expressions for the Yukawa matrices and deduced flavour parameters of the model in terms of the underlying VEVs $\langle S \rangle$ and $\langle T' \rangle$. However, we are not able to solve the derived relations, such as e.g. Eq. (3.8), analytically for s and t' . In other words, we cannot parameterize the flavour signatures of the high-energy model using the physically known low-energy flavour parameters, i.e. the quark masses $m_i^{u,d}$ and the CKM mixing V_{CKM} .

On the other hand, it is possible to invert the approximate formula of Eq. (2.11) numerically. Doing so, we encounter the technical complication of multiple solutions, as already mentioned at the end of Section 2.3. Moreover, starting from a left-right symmetric theory the right-chiral up-type and down-type quark sector cannot be rotated independently. This enforces the introduction of the mixing matrix U'_{CKM} which parameterizes the coupling of the W'^{\pm} bosons to the right-chiral quarks and contains six physical phases. As both the mixing matrix U'_{CKM} as well as the appropriate choice of a solution are unknown, we choose to scan over these degrees of freedom. In this section, we describe the technical details of our procedure. In principle a scan of the parameter space should be performed over all parameters of the model, namely s , t' , λ , $\tan \beta = v_u/v_d$ and M . However, as s and t' feature large hierarchies a direct scan over these is not reasonable. Thus we use the alternative ansatz and scan over so-called “adapted flavour parameters” which we define in the following. We point out that these are deduced from the parameters of the SM Yukawa couplings.

\tilde{m}_u	$0.5 - 2.9 \text{ MeV}$	\tilde{m}_d	$1.2 - 4.8 \text{ MeV}$	$\tilde{\theta}_{12}^L$	$12.89^\circ - 13.19^\circ$
\tilde{m}_c	$0.53 - 0.71 \text{ GeV}$	\tilde{m}_s	$30 - 78 \text{ MeV}$	$\tilde{\theta}_{23}^L$	$1.54^\circ - 2.56^\circ$
\tilde{m}_t	$162 - 288 \text{ GeV}$	\tilde{m}_b	$2.78 - 4.44 \text{ GeV}$	$\tilde{\theta}_{13}^L$	$0.101^\circ - 0.28^\circ$

Table 2: Ranges of the adapted flavour parameters over which the scan is performed. The mixing angles $\tilde{\theta}_{ij}^{R}$ of U'_{CKM} are varied in their full range $[0^\circ, 90^\circ]$ and additionally in a reduced range $[0^\circ, 1.5^\circ]$. All phases are varied between 0 and 2π .

4.1 Adapted flavour parameters

We start our considerations with the quark masses and mixings as fitted in the SM framework [66]. In order to take into account the physical but experimentally unknown mixing of the right-chiral quarks in the $SU(2)'$ charged current, we also add mixing angles and phases for the matrix U'_{CKM} . With this input we calculate an explicit numerical realization for the 3×3 matrices Y_u and Y_d in an arbitrary basis. For a given such pair it is possible to invert Eq. (2.11), thereby deriving s and t' numerically, see Appendix B. As explained in Section 2.3, these are however only approximations, and we expect sizeable corrections for the third generations. Nevertheless they provide a well-motivated starting point for the exact computation.

Inserting the so-derived numerical values of s and t' into the 9×9 mass matrix of Eq. (3.3), we can diagonalize \mathcal{M}^u (and likewise \mathcal{M}^d) explicitly. As our experimental knowledge is limited to the three generations of light quarks, it is sufficient to focus on the upper left 3×3 blocks of both the full mass matrices as well as the associated mixing matrices. Comparing these with the input parameters, we find that the masses and mixing angles related to the third generation are systematically too small. We therefore adjust the input parameters such that the effective 3×3 Yukawa matrices of the full theory match the matrices Y_u and Y_d of the SM. We denote these adjusted input parameters as “adapted flavour parameters” (labelled by a tilde), and define ranges (given in Table 2) over which we perform the scan.

4.2 Details of the scan

Having defined the adapted flavour parameters we describe in detail our systematic scan over possible flavour effects. We do not claim this scan to be exhaustive as the procedure may systematically exclude allowed regions of the underlying parameter space. Nevertheless, it provides important insights into the essential flavour effects of this model. The scan itself is performed using the following steps.

1. Randomly generate a point in the space of adapted flavour parameters where the allowed ranges are given in Table 2. Furthermore, choose also random values for $\lambda \in [1.5, 3]$, $\tan \beta \in [1, 15]$ and $M \in [750, 2500] \text{ GeV}$.
2. Calculate s and t' by inverting Eq. (2.11) using the procedure described in Appendix B. Here we randomly choose one of the eight solutions.

3. Insert the so-derived s and t' as well as λ , $\tan\beta$ and M into the full 9×9 mass matrices $\mathcal{M}^{u,d}$ and diagonalize these numerically.
4. Deduce the effective SM-like Yukawa parameters for the three light generations, i.e. $m_i^{u,d}$ and $V_{\text{CKM}}^{\text{eff}}$.
5. Compare these with the experimentally allowed 3σ ranges.⁶ In case of agreement, save the point $(s, t', \lambda, \tan\beta, M)$ as a viable choice of input parameters.

Following these steps, we have generated about 3,000 viable points using the full range of adapted parameters. However, scanning the full parameter space of the mixing angles $\hat{\theta}_{ij}^R$ of U'_{CKM} is rather inefficient as only a small fraction of all points turns out to be physically acceptable. For this reason, we have additionally performed a more extensive scan where we choose random values of $\tilde{\theta}_{ij}^R$ within the small interval $[0^\circ, 1.5^\circ]$. The resulting 30,000 viable points differ qualitatively from the full scan only in U_{CKM} , i.e. the coupling of the right-chiral quarks to the W^\pm bosons. In order to enhance the statistics, we have combined both sets of points in our analysis (unless we are interested in the results for U_{CKM} itself).

Before turning to the presentation and discussion of the physical results of our scan, we comment on the qualitative structure of the flavon VEVs $\langle S \rangle$ and $\langle T' \rangle$. In the original GRV model [39], the flavon VEVs can be derived from the SM Yukawa matrices via the approximate relation $\langle S \rangle \propto Y^{-1}$. This simple relation entails that the flavon VEVs directly inherit the hierarchies of the Yukawa matrices in an inverse way. In contrast to this, the situation in our PS flavour model is more involved. Due to the linear combination of the VEVs $\langle S \rangle$ and $\langle T' \rangle$ in Eq. (2.11), a simple direct relation of the hierarchies in the SM Yukawas and the flavon VEVs does not exist. While many viable points of the scan do indeed feature flavon VEVs with hierarchies similar to those of the inverse Yukawas, there exists a significant number of points where the hierarchies of VEVs is less (or more) pronounced. Similarly, the mixing angles describing the mismatch of the matrices s and t' can in some cases be significantly larger than those of the CKM matrix.

5 Quark flavour phenomenology

In this section, we discuss the physical implications of our PS flavour model. Starting from the adapted flavour parameters together with the ranges for λ , $\tan\beta$ and M as defined in Section 4, we observe that the values of $\tan\beta$ and M corresponding to the viable points are equally distributed throughout the full allowed ranges. In contrast to this, the parameter λ does not cover the full allowed range but only $\lambda \in [1.5, 2.5]$. In fact, it peaks around $\lambda = 2$, which is exactly the value we have used to determine the ranges of the adapted flavour parameters. In principle, we could have expanded our scan by additionally deriving adapted flavour parameters for other values of λ , thereby enlarging

⁶We consider the masses at the electroweak scale, i.e. $m_i^{u,d}(M_Z)$ [67], and the experimental constraints on the absolute values of the individual CKM entries (not those obtained from additionally demanding unitarity of the CKM matrix).

the intervals in Table 2. However, we refrain from doing so as we are mainly interested in this part of the parameter space.⁷

Regarding the M -dependence of all physical results, we note that this has been factored out in the definition of the flavour breaking VEVs of Eq. (2.6). Following this parameterization, the approximate Yukawa relations of Eq. (2.11) do not explicitly depend on M . Likewise, we do not expect any explicit M -dependence of the 3×3 matrices $a \dots f$, cf. Eq. (3.6). On the other hand, an implicit M -dependence may in principle be induced via the intricate procedure of determining s and t' , in particular for the third generation of quarks. We have therefore checked for such a possibility in our scan. However, no extra (implicit) dependence on M is found in any of the quantities, at least above a threshold of $M \sim 1$ TeV. This observation allows us to understand the dependence on the scale M explicitly throughout the model, particularly in all corrections.

As an application of this fact, we may limit our discussion of characteristic flavour effects to a narrower mass band. In some of the following studies we choose this to be $M \in [1, 1.2]$ TeV, which reduces our set to approximately 3,500 viable points. This restriction clarifies the dependence of physical observables on the other input parameters of the scan as it reduces the spread due to the variation of M . The results obtained for this reduced mass band may afterwards be used to extrapolate the effects to larger values of M using the explicitly known M -dependence. Reversely, we can also use the explicit M -dependence to rescale all generated points to a single mass scale. We make use of such a rescaling in the discussion of U_{CKM} in Section 5.4 in order to increase the statistics.

5.1 Effective SM flavour parameters

When defining the ranges of the adapted flavour parameters, we have aimed at choices which entail a coverage of the complete range of experimentally allowed Yukawa parameters. This turns out to be possible for most of the parameters, however, not all of them are distributed equally over the allowed range.

Especially the absolute values of the CKM elements $|V_{tb}|$, $|V_{ts}|$, $|V_{cs}|$ and $|V_{cd}|$ are more constrained in our setup. This can be traced back to fact that the direct bounds on these CKM elements are relatively weak while the correction ΔV_{CKM} (related to non-unitarity) is small. If we instead compare the covered range to the CKM elements as deduced from the SM fit assuming unitarity [68, 69], we generate many points outside the 3σ region. In particular, we find that our $|V_{tb}|$ is typically smaller. The experimental bounds we impose on the individual CKM elements, the ranges deduced from the SM fit and the ranges covered in our scan are all given in Table 3 for comparison. Concerning the masses $m_i^{u,d}$ we find that they all cover the full allowed range [67]. However, there is a tendency to lower values especially for the charm mass. For the light quark masses, we also see a deficit in the largest values of the allowed ranges, although not as pronounced as for the charm mass. We interpret these effects as relics of our scan, as the setup of the model generally lowers the masses. The allowed ranges for the masses can be found in Table 4.

Having checked that the model is capable of generating the flavour structure of the SM, we now turn our attention to quark flavour effects beyond the Standard Model.

⁷In the one generation case it is possible to show that $\lambda \gtrsim \sqrt{2}$, and larger values are disfavoured in a perturbative theory.

	$ V_{ud} $	$ V_{us} $	$ V_{ub} $
experiment	0.9736 – 0.9749	0.2229 – 0.2277	0.0027 – 0.0056
unitarity	0.9739 – 0.9747	0.2235 – 0.2272	0.0031 – 0.0040
covered	0.9737 – 0.9748	0.2231 – 0.2277	0.0027 – 0.0056
	$ V_{cd} $	$ V_{cs} $	$ V_{cb} $
experiment	0.2010 – 0.2490	0.9380 – 1.0340	0.0372 – 0.0450
unitarity	0.2234 – 0.2271	0.9730 – 0.9739	0.0378 – 0.0450
covered	0.2229 – 0.2276	0.9727 – 0.9741	0.0372 – 0.0450
	$ V_{td} $	$ V_{ts} $	$ V_{tb} $
experiment	0.0066 – 0.0102	0.0319 – 0.0481	0.9250 – 1.1170
unitarity	0.0079 – 0.0099	0.0372 – 0.0438	0.9990 – 0.9993
covered	0.0066 – 0.0102	0.0355 – 0.0447	0.9711 – 0.9992

Table 3: Coverage of the allowed range of $|(V_{\text{CKM}}^{\text{eff}})_{ij}|$. The first line corresponds to the direct experimental limits we impose for the scan [66]. The second line shows the allowed range deduced from the SM fit assuming unitarity of the CKM matrix [66]. The last line corresponds to the range covered in our scan.

m_u	0.5 – 2.9 MeV	m_d	1.2 – 4.8 MeV
m_c	0.53 – 0.71 GeV	m_s	30 – 78 MeV
m_t	162 – 180 GeV	m_b	2.78 – 2.96 GeV

Table 4: Ranges of the quark masses $m_i^{u,d}$ covered in the scan.

5.2 Masses of the new heavy quarks

The masses of the heavy up-type quark partners can be read off from the approximately diagonalized mass matrix of Eq. (3.7). A similar expression can be deduced for the down-type quark partners by replacing the index u by d . As we have explicitly factored out the mass scale M it is reasonable to consider only the mass ratio

$$\mu_F = \frac{m_F}{M}. \quad (5.1)$$

With the matrix \hat{f} being independent of isospin, we can directly infer that one set of heavy up-type partners equals one set of down-type partners in mass, denoted by U_i'' and D_i'' in the following, where U_i (D_i) are the three generations of up-type (down-type) quarks. This observation is numerically verified in our scan, where the corresponding masses are equal at the sub-percent level. Introducing a VEV $\langle T \rangle \neq 0$ for the $SU(2)$ triplet flavon T would break this mass degeneracy by an amount proportional to $\langle T \rangle$. Being proportional to $\hat{e}_{u,d}$, the masses of the other set of heavy quark partners, denoted by U_i' and D_i' , will generally depend on isospin.

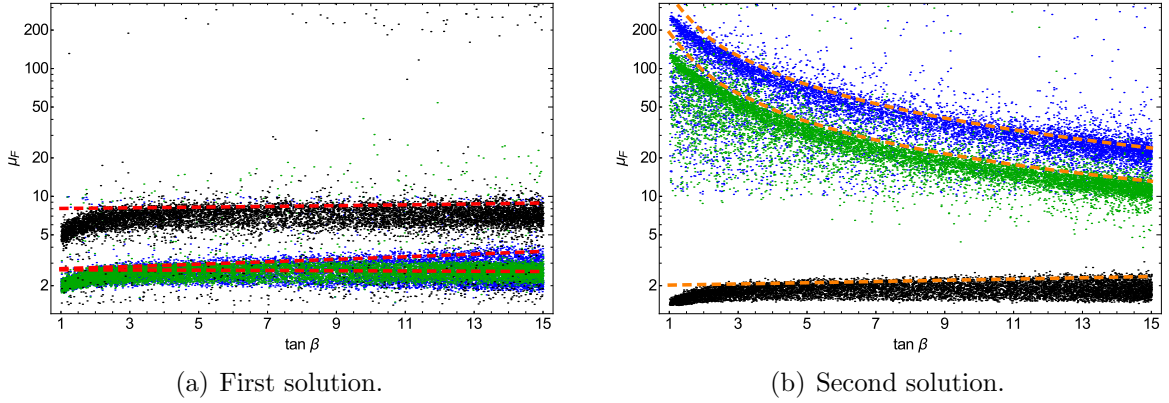


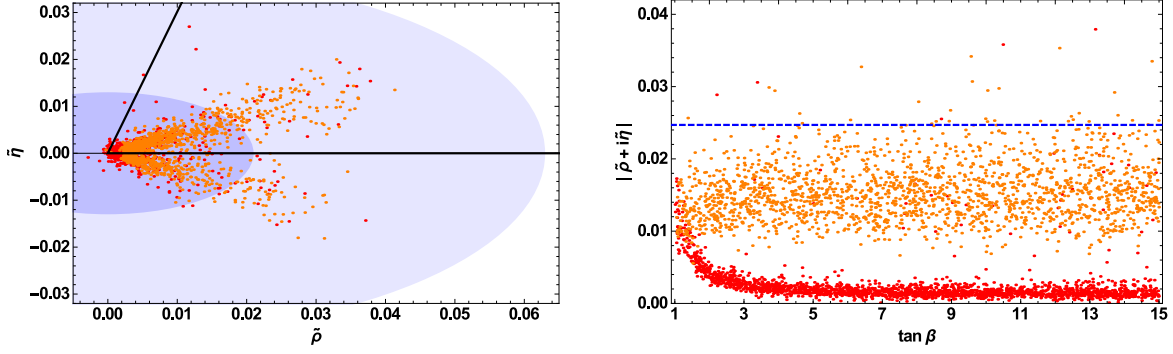
Figure 3: Mass ratios μ_F of the lightest generation of heavy quark partners with respect to $\tan\beta$. The plots show the masses of the first top partner in black, the first bottom partner in blue, and the second top and bottom partners in green. The two solutions of Eq. (2.12) are given for each mass ratio as dashed lines in red (a) and orange (b), respectively.

Focusing on the lightest generation of heavy quark partners, i.e. t' , b' , t'' and b'' , the multiplicity of solutions to Eq. (2.11) is dominated by the multiplicity of the one generation case, see Eq. (2.12). The scan therefore generates two distinct bands for each of the four mass ratios μ_F . These in turn depend on $\tan\beta$, which can be traced back to the appearance of y_u and y_d in Eq. (2.12). The resulting $\tan\beta$ -dependence of the heavy quark masses calculated from the one generation case fits the results of the scan reasonably well as illustrated in Figure 3. Here, we have plotted the mass ratios μ_F of the four lightest quark partners (t' , b' , t'' and b'') against $\tan\beta$. For clarity we have separated the two possible solutions. The mass ratios of t'' and b'' are shown in green (as both are equal), the one of t' in black and that of b' in blue. Additionally, we have plotted the $\tan\beta$ -dependence of the mass ratios deduced from Eq. (2.12) where we have used the central values of the SM Yukawa couplings and $\lambda = 2$ as fixed input. Here, we introduce a colour coding for this and the following plots: masses belonging theoretically to the first (second) solution of Eq. (2.12) are shown in red (orange).

We can conclude from the plots of Figure 3 that the mass ratios μ_F of the heavy quark partners may be of order one, and thus their masses can be in the TeV-regime. However, depending on the solution, we may expect either a set of three quark partners (b' , t'' and b'') within a small mass range or solely the top partner t' to appear in experiments. This shows that the two solutions differ qualitatively in their phenomenological predictions. We will encounter further differences in the following discussions.

5.3 Non-unitarity of $V_{\text{CKM}}^{\text{eff}}$

Due to the $\epsilon_{u,d}^2$ -dependent contribution ΔV_{CKM} to the effective CKM matrix, see Eq. (3.15), the coupling of the W^\pm bosons to the three generations of light quarks is no longer described by a unitary matrix. This non-unitarity can be quantified by studying the unitarity triangles constructed from $V_{\text{CKM}}^{\text{eff}}$. For the sake of clarity, we limit our discussion



(a) The origin of the standard unitarity triangle. The blue-shaded regions correspond to the 1σ and 3σ uncertainty of the measured SM Wolfenstein parameters $\bar{\rho}$ and $\bar{\eta}$ [66].

(b) The absolute value of $\tilde{\rho} + i\tilde{\eta}$ plotted against $\tan\beta$ for points with $M \in [1, 1.2]$ TeV. The dashed blue line indicates the corresponding 1σ error of $|\bar{\rho} + i\bar{\eta}|$ as obtained in the SM [66].

Figure 4: The non-unitarity of $V_{\text{CKM}}^{\text{eff}}$. For the first (second) solution of Eq. (2.12), we show $\tilde{\rho} + i\tilde{\eta}$, i.e. the measure of the deviation from unitarity, in red (orange).

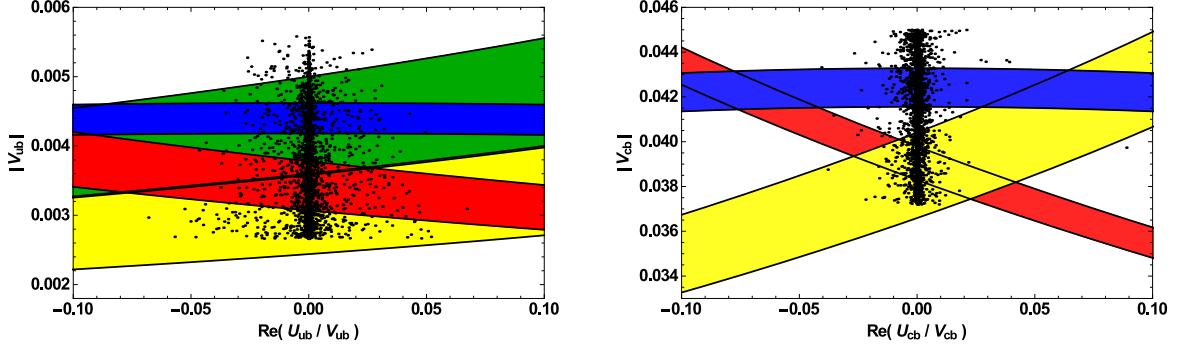
to the “standard unitarity triangle”. However, we have checked that the other unitarity triangles lead to analogous results with similar or smaller effects.

Generically we do not expect large deviations from the SM as we have limited our scan to points which are compatible with the absolute values of the CKM matrix elements, taking into account the uncertainty of the measurements. This is a simplifying assumption as the determination of the CKM elements from experimental measurement is also affected by the couplings of the right-chiral quarks. To give a complete picture, we would have to redo the extraction of the CKM elements in the presence of additional couplings of right-chiral quarks (U_{CKM}) and without the assumption of unitarity. Clearly, such an explicit fit is beyond the scope of our current work.

In order to quantify the non-unitarity of $V_{\text{CKM}}^{\text{eff}}$ via the standard unitarity triangle, we define the complex quantity

$$\tilde{\rho} + i\tilde{\eta} \equiv \frac{V_{ub}V_{ud}^* + V_{cb}V_{cd}^* + V_{tb}V_{td}^*}{V_{cb}V_{cd}^*}, \quad (5.2)$$

whose deviation from zero is a measure of the deviation from unitarity. In Figure 4, we show $\tilde{\rho} + i\tilde{\eta}$ for the complete set of viable points at the origin of the unitarity triangle. In addition, we present the $\tan\beta$ -dependence of its absolute value $|\tilde{\rho} + i\tilde{\eta}|$, where we limit ourselves to viable points which lie in the mass band $M \in [1, 1.2]$ TeV for the sake of clarity. The points associated with the two solutions are again distinguished by the colour code introduced above. We compare these results of our scan with the 1σ and 3σ uncertainties of the measured SM Wolfenstein parameters $\bar{\rho}$ and $\bar{\eta}$ [66]. As expected, the deviation from unitarity predicted in our scan is within the SM uncertainties. Moreover, we again find that the size of this effect depends crucially on the type of solution. This is particularly apparent in the $\tan\beta$ -dependence of $|\tilde{\rho} + i\tilde{\eta}|$, cf. Figure 4(b). Here, the second (orange) solution is basically independent of $\tan\beta$ whereas the first (red) is of similar size for $\tan\beta = 1$, but becomes negligible for $\tan\beta \gtrsim 3$. Thus, the effect can be practically absent even for small values of the flavour breaking mass scale M . Considering the values of $\tilde{\rho} + i\tilde{\eta}$ in the complex plane near the origin of the unitarity triangle, we observe that



(a) Impact of U_{ub} on the determination of $|V_{ub}|$ as given in [72]. The coloured bands show different measurements: inclusive decays (blue), $B \rightarrow \pi l \nu$ (red), $B \rightarrow \rho l \nu$ (yellow), $B \rightarrow \tau \nu$ (green). The points obtained in our scan are shown as black dots.

(b) Impact of U_{cb} on the determination of $|V_{cb}|$ as given in [72]. The coloured bands show different measurements: inclusive decays (blue), $B \rightarrow D^* l \nu$ (red), $B \rightarrow D l \nu$ (yellow). The points obtained in our scan are shown as black dots.

Figure 5: The impact of U_{CKM} on the determination of $|V_{\text{CKM}}|$. Using the explicit M -dependence, the points of our scan have been scaled to the reference scale $M = 1 \text{ TeV}$.

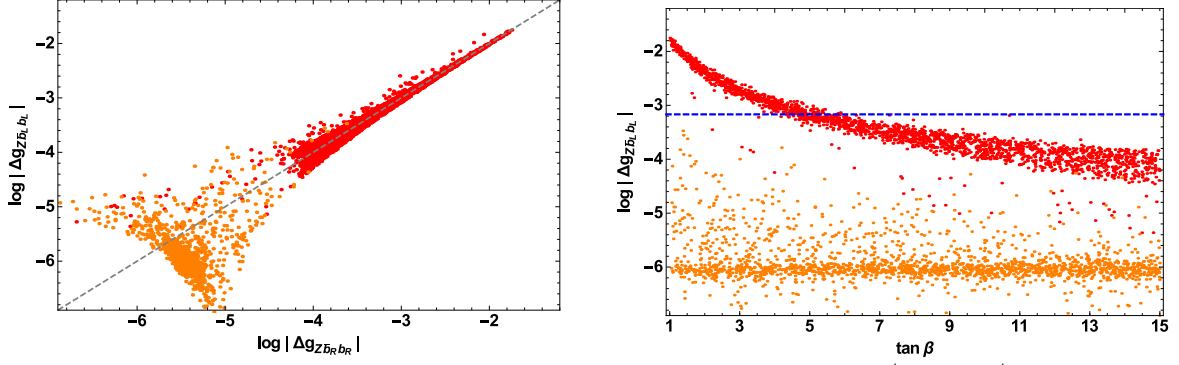
the real part $\tilde{\rho}$ is generically positive, cf. Figure 4(a). This indicates that the effect is dominated by the decrease of $|V_{tb}|$ which in turn reduces the length of the upper right line of the unitarity triangle.

5.4 Coupling of right-chiral quarks to W^\pm via U_{CKM}

As described in Section 3.2, the light generations of right-chiral quarks couple to the SM W^\pm gauge boson due to the mixing of q_R with Ξ_R in Eq. (2.4). The corresponding coupling strength is parameterized by U_{CKM} as stated explicitly in Eq. (3.15c). Formally it is proportional to $\epsilon_{u,d}^2$ which we find confirmed in our scan. Furthermore, we see no direct correlation between U_{CKM} and V_{CKM} . The existence of such a coupling modifies the determination of the CKM elements from experimental data. In particular, it might be significant in view of the puzzling tension between the determination of $|V_{ub}|$ and $|V_{cb}|$ from exclusive and inclusive B -meson decays within the SM [66, 70]. The additional couplings U_{ub} and U_{cb} of right-chiral quarks to W^\pm can in principle reduce (though not completely resolve) this tension as the inclusive decay is proportional to $|V_{xb}|^2 + |U_{xb}|^2$, while the exclusive decay is proportional to $|V_{xb} \pm U_{xb}|^2$, see e.g. the discussions in [71–73]. Yet, from the point of view of our model, our scan may reveal which experimental measurements are “theoretically preferred”.

In our scan, we have searched for such effects, but do not find a conclusive answer. Figure 5 shows the 1σ regions of $|V_{ub}|$ and $|V_{cb}|$ as a function of U_{ub} and U_{cb} [72]. We have additionally plotted the 3,000 points of our scan over the full parameter range, scaled to the reference mass scale $M = 1 \text{ TeV}$. As a result we find that the relative contributions of U_{CKM} are at the percent level at most. Furthermore, the scan shows no preference for any of the measurements, and no apparent correlation between U_{ub} and U_{cb} is seen.

⁸Here the sign is determined by the currents (axial or vector) mediating the decay.



(a) Correlation between the coupling of the Z boson to the left- and right-chiral bottom quark. The dashed grey line indicates the diagonal.

(b) The dependence of $|\Delta g_{Z\bar{b}_L b_L}|$ on $\tan \beta$. The dashed blue line indicates the 3σ limit of Eq. (5.3) (points below are allowed).

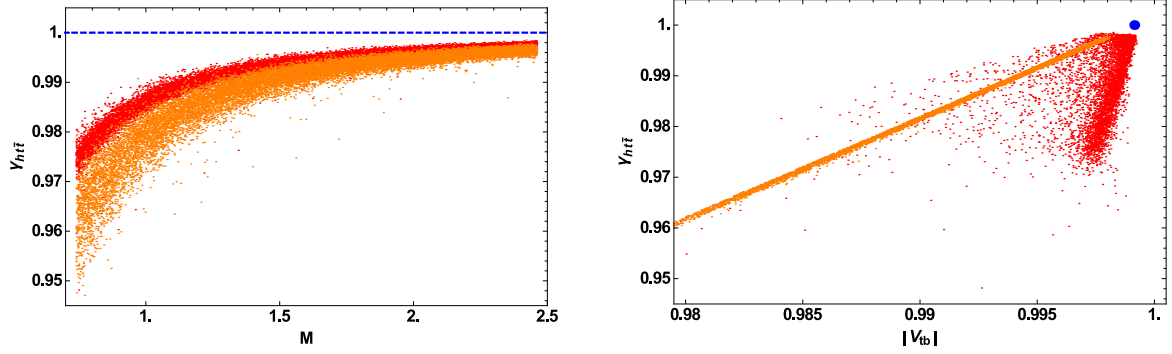
Figure 6: Correction of the Z boson coupling to the b quark. In red (orange) we show the points corresponding to the first (second) solution of Eq. (2.12) for the mass band $M \in [1, 1.2]$ TeV.

5.5 Anomalous Z coupling

As can be seen explicitly in Eq. (3.14), the coupling of the Z boson to the left- and right-chiral quarks is modified as well. Similarly to the effects discussed above, the largest deviation arises in the top quark coupling, where it is in the range of a few percent for moderate values of M . Experimentally, the Z -top-top coupling cannot be determined directly from the decay of an on-shell Z boson as it is kinematically forbidden. Thus top physics processes such as $t\bar{t}Z$ production at the LHC [74], or the production of a pair of top quarks mediated by the neutral gauge bosons Z^* and γ^* at the ILC [75] provide alternative and promising ways of measuring the coupling of the Z to the top quark. However, as the resulting bounds are expected to be relatively weak, we focus on the coupling of the Z to the bottom quark. This decay has been measured precisely at LEP2 [76] with $\Gamma(Z \rightarrow b\bar{b}) \approx 375.87 \pm 0.17$ MeV [66]. It involves the couplings of both the left- as well as the right-chiral b quarks. Considering the correlation of their corrections within our model, plotted in Figure 6(a), we observe that $|\Delta g_{Z\bar{b}_L b_L}|$ and $|\Delta g_{Z\bar{b}_R b_R}|$ are roughly of equal size, unless the values are small and thus negligible for phenomenological purposes. We can therefore make the simplifying assumption that both corrections are approximately identical. Assuming furthermore that the correction to the $Z\bar{b}b$ coupling is within the experimental uncertainty, we can set the following 3σ limit on the couplings,

$$|\Delta g_{Z\bar{b}_L b_L}| \sim |\Delta g_{Z\bar{b}_R b_R}| \lesssim 6.8 \times 10^{-4}. \quad (5.3)$$

This bound reduces the number of viable points of the scan by roughly 10 percent. The so-excluded points all belong to the first solution of Eq. (2.12). Assuming $M \in [1, 1.2]$ TeV, Fig. 6(b) shows the $\tan \beta$ -dependence of $|\Delta g_{Z\bar{b}_L b_L}|$ for both solutions. While the second (orange) solution does not vary with $\tan \beta$, the first (red) is characterized by decreasing values of $|\Delta g_{Z\bar{b}_L b_L}|$ for increasing $\tan \beta$. Thus, the bound of Eq. (5.3) is satisfied more often for larger values of $\tan \beta$, and all model points corresponding to the first solution with $\tan \beta \lesssim 4$ can be excluded (yet smaller values are allowed for larger M).



(a) The normalized coupling $\gamma_{h\bar{t}t}$ as a function of M . The SM expectation is shown by the dashed blue line. The error of the experimental direct measurement exceeds the plotted range.

(b) Correlation of the normalized coupling $\gamma_{h\bar{t}t}$ and $|V_{tb}|$. The point corresponding to the SM value is shown in blue. The experimental errors on both quantities exceed the plotted ranges.

Figure 7: Correction of the normalized Higgs-top-top coupling $\gamma_{h\bar{t}t}$. In red (orange) we show the points corresponding to the first (second) solution of Eq. (2.12).

5.6 Anomalous Higgs coupling

Following the discussion of Section 3.3, the Higgs coupling to the top quark $g_{h\bar{t}t}$ can receive sizeable corrections in our setup. However, such an effect is negligible already for the b quark as well as for all lighter quarks. Being of order ϵ_u^2 , see Eq. (3.17), the correction to $g_{h\bar{t}t}$ reduces drastically for increasing M . In order to visualize the deviation from the SM, it is useful to normalize the coupling $g_{h\bar{t}t}$ to its SM expectation $\sqrt{2}m_t/v_u$. To this end, we define

$$\gamma_{h\bar{t}t} = \frac{g_{h\bar{t}t} v_u}{\sqrt{2} m_t}. \quad (5.4)$$

The plot in Figure 7(a) shows that the deviation of this quantity from its SM value is of the order of a few percent for small values of M . Experimentally, the Higgs-top-top coupling is however only poorly known with an uncertainty of about 30 percent [77–79]. The correction to $\gamma_{h\bar{t}t}$ is therefore expected to be more important for precision observables, where the top quark and the Higgs appear in loops so that indirect constraints apply.

Searching for correlations, we find that $\gamma_{h\bar{t}t}$ and $|V_{tb}|$ show a similar M -dependence for the points corresponding to the second (orange) solution of Eq. (2.12), cf. Figure 7(b). Such a correlation can be of phenomenological interest as the top quark decays nearly instantaneously into a bottom quark and a W boson. For smaller values of M , it thus amplifies the reduction of associated Higgs production, $gg \rightarrow t\bar{t}H$, a process currently searched for at the LHC [80,81]. In contrast to this, the first (red) solution of Eq. (2.12) does not feature such a correlation.

Besides the reduction of the normalized coupling $\gamma_{h\bar{q}q}$, we also obtain flavour changing couplings of the Higgs boson which can be relevant for flavour changing neutral currents (FCNC). The corresponding weak experimental bounds for heavy quarks will eventually become stricter. A detailed analysis of FCNC effects, including the Z boson coupling, is therefore well motivated but beyond the scope of this paper. Concerning the light quarks, for which strict bounds on FCNC exist, we stress that these are naturally suppressed in our PS flavour model.

6 Conclusion

Combining the idea of vertical and horizontal unification, we have constructed a Pati-Salam symmetric model with gauged $SU(3)_I \times SU(3)_{II}$ flavour symmetry. In the unbroken phase, the model is characterized by an explicit left-right (i.e. Z_2) symmetry and an electroweak symmetry breaking Higgs bi-doublet. Analogous to the construction of Grinstein, Redi and Villadoro (GRV), the flavour structure of the SM quarks and leptons originates in a renormalizable Lagrangian involving new heavy fermions as well as a set of scalar flavon fields. Vacuum expectation values of the latter generate masses for the additional fermions, which in turn mediate the associated flavour symmetry breaking to the SM fermions in a seesaw-like fashion. In contrast to GRV, our left-right symmetric PS setup requires the introduction of two (rather than one) heavy fermionic partners for each SM fermion. As a consequence, the cancellation of flavour gauge anomalies entails a further extension of the fermionic particle content. This finds a natural realization in the lepton sector where light Majorana neutrino masses can be generated by introducing PS neutral fermions which acquire large Majorana masses from another set of flavon fields. These flavons break the flavour symmetry completely at a very high scale so that all flavour gauge bosons decouple from low-energy physics.

In the quark sector, the effective SM Yukawa matrices are related to the VEVs of the flavon fields neither linearly as in the MFV approach nor in a simple inverse way as in the original GRV setup. The approximate relations, obtained by integrating out the heavy fermions and given in Eq. (2.11), do not fix the flavon VEVs uniquely. Besides the unknown mixing of the right-chiral quarks (which is physical in our PS model), there exists a total of eight solutions for the flavon VEVs, all giving the same approximate SM Yukawa matrices. Inserting these vacua into the complete fermion mass matrices, it is possible to extract the masses and the mixing angles of the three generations of SM quarks. Comparing these with the physical values, we find that the approximate formulas of Eq. (2.11) do not adequately describe the third generation. Such a behaviour is expected and can be traced back to substantial mixing of the third generation of quarks with the corresponding heavy fermionic partners. In order to correct for this effect, we define adapted flavour parameters and take these as input for our numerical scan. Similarly to the GRV case, the construction of the model guarantees that non-standard flavour transitions between the first and the second generation are highly suppressed, while new physics effects involving the third generation of quarks are expected to be phenomenologically relevant. Characteristic effects include the non-unitarity of the effective CKM matrix, the coupling of the SM right-chiral quarks to the electroweak W^\pm boson and anomalous couplings of the Z as well as the Higgs boson to two SM quarks. Quantitatively, all these effects are of order $\epsilon_{u,d}^2$, where $\epsilon_{u,d} = \langle h_{u,d}^0 \rangle / M$ denotes the ratio of the Higgs VEV over the sole explicit mass scale M of the model. By construction, M corresponds to the scale of the lightest fermionic partners, and we choose it to be in the TeV regime. The discussed new physics signatures of our PS GRV setup are therefore below the current experimental sensitivity. Yet, depending on the type of solution for the flavon VEVs, the phenomenological predictions beyond the SM might be tested in the near future.

In this work we have not addressed the question of the underlying dynamics which governs the vacuum structure of the flavon fields. In our numerical scan we find that

viable flavon VEVs feature hierarchical patterns which are more or less comparable to those of the inverse Yukawa matrices. Ideas of generating hierarchical flavon VEVs from an appropriate flavour-invariant scalar potential have already been discussed in the context of MFV, and we intend to apply similar methods of spontaneous flavour symmetry breaking to our PS GRV setup in a future publication. Another subject of further investigation concerns the lepton sector. In this work, we have presented a neutrino extension in which the flavour structure of the neutrinos decouples from the hierarchical patterns of the quark sector. The construction of a fully realistic charged lepton sector, including a detailed discussion of lepton-flavour violating processes and lepton non-universality, is left for future work.

Acknowledgements

This work is supported by the Deutsche Forschungsgemeinschaft (DFG) within the Research Unit FOR 1873 (Quark Flavour physics and Effective field Theories). FH acknowledges support from the Naturwissenschaftlich-Technische Fakultät, University of Siegen.

Appendix

A Lepton sector

A.1 Neutrinos

In order to accommodate Majorana neutrinos, we have extended the Pati-Salam GRV model by $\mathcal{L}_{\text{Yuk}}^\nu$ of Eq. (2.5). Integrating out the Majorana fermions $\bar{\Theta}_L$ and Θ_R generates an effective heavy Majorana mass for Σ_R^ν , cf. Eq. (2.13). This induces a Majorana mass term for the left-chiral neutrino \bar{q}_L^ν via the terms of Eq. (2.4). In the first part of this appendix, we derive the structure of the resulting neutrino mass matrix. In the second part, we discuss an alternative ansatz in which q_R^ν (rather than Σ_R^ν) acquires a heavy Majorana mass. This is one of several alternative examples leading to light neutrino masses via Eq. (2.4). The flavour structure of the resulting mass matrix is, however, less attractive as will be discussed exemplarily below.

A.1.1 Preferred neutrino extension

Starting with the neutral part of the Lagrangian of Eq. (2.3), it is straightforward to integrate out the heavy fields $\Theta_{L,R}$ and $\Xi_{L,R}$. Inserting the flavon and Higgs VEVs we find

$$\begin{aligned} \mathcal{L}_{\text{mass}}^\nu = & \lambda \bar{q}_L^\nu \frac{v_u}{\sqrt{2}} \Sigma_R^\nu + M \bar{\Sigma}_L^\nu t_u \Sigma_R^\nu + M \bar{\Sigma}_L^\nu q_R^\nu + h.c. \\ & - \lambda \frac{v_u}{\sqrt{2}} \bar{q}_L^\nu s^{-1} q_R^\nu + h.c. \\ & - \frac{1}{2} \Sigma_R^\nu M_{\Sigma_R^\nu} \Sigma_R^\nu + h.c., \end{aligned} \tag{A.1}$$

with $M_{\Sigma_R^\nu} = \frac{(\varphi'_\alpha \Lambda_\varphi)^2}{\Lambda_\nu} s_\nu^{-1}$, cf. Eq. (2.13). To arrive at this simple intermediate result, we have assumed $\frac{M^2}{\Lambda_\nu^2} \ll \Lambda_\nu$. Next, we integrate out Σ_R^ν to obtain

$$\begin{aligned} \mathcal{L}_{\text{mass}}^\nu &= \frac{\Lambda_\nu}{2(\varphi'_\alpha \Lambda_\varphi)^2} \left(\lambda \frac{v_u}{\sqrt{2}} \bar{q}_L^\nu + M \bar{\Sigma}_L^\nu t_u \right) s_\nu \left(\lambda \frac{v_u}{\sqrt{2}} \bar{q}_L^\nu + M \bar{\Sigma}_L^\nu t_u \right)^T + h.c. \\ &\quad + M \bar{\Sigma}_L^\nu q_R^\nu - \lambda \frac{v_u}{\sqrt{2}} \bar{q}_L^\nu s^{-1} q_R^\nu + h.c. , \end{aligned} \quad (\text{A.2})$$

where we have separated the Majorana mass term in the first line from the Dirac terms in the second line. $\bar{\Sigma}_L^\nu$ and q_R^ν form a Dirac pair and can be integrated out simultaneously. It is interesting to note that already the equation of motion of q_R^ν is sufficient to deduce the effective light neutrino mass term. Inserting $\bar{\Sigma}_L^\nu \rightarrow \lambda \frac{v_u}{\sqrt{2}M} \bar{q}_L^\nu s^{-1}$ yields

$$\mathcal{L}_{\text{mass}}^\nu = \frac{1}{2} \bar{q}_L^\nu \left[\frac{\Lambda_\nu v_u^2 \lambda^2}{2(\varphi'_\alpha \Lambda_\varphi)^2} (\mathbb{1} + s^{-1} t_u) s_\nu (\mathbb{1} + s^{-1} t_u)^T \right] \bar{q}_L^{\nu T} , \quad (\text{A.3})$$

which corresponds to the effective mass matrix reported in Eq. (2.14). Following this derivation, the occurrence of the second term in the sum $(\mathbb{1} + s^{-1} t_u)$ is traced back to the coupling of Σ_R^ν to \bar{q}_L^ν via $\bar{\Sigma}_L^\nu$ and q_R^ν , cf. Eq. (A.1).

It is important to note that a high scale VEV $\langle S'_\nu \rangle$ is essential. A vanishing or too small value would imply only a small Majorana mass for Θ_R as well as a mixing with Σ_R^ν . Integrating out the heavy fields Σ_R^ν , $\bar{\Sigma}_L^\nu$ and q_R^ν results in a strongly hierarchical Dirac mass term for \bar{q}_L^ν and Θ_R which is phenomenologically excluded, unless the Majorana contribution, identical to Eq. (2.14), to the neutrino mass dominates.

A.1.2 An alternative neutrino extension

Altering the flavour quantum numbers of Φ & Φ' from $(\mathbf{8}, \mathbf{1})$ & $(\mathbf{1}, \mathbf{8})$ to $(\mathbf{3}, \bar{\mathbf{3}})$ & $(\mathbf{3}, \bar{\mathbf{3}})$, entails a slightly modified form of $\mathcal{L}_{\text{Yuk}}^\nu$ in Eq. (2.5): the Z_2 pair $(\bar{\Xi}_L, \Sigma_R)$ simply gets replaced by (\bar{q}_L, q_R) . Analogous to the preferred case, one obtains a Majorana mass term for q_R^ν after integrating out $\Theta_{L,R}$.

$$\begin{aligned} \mathcal{L}_{\text{mass}}^\nu &= \lambda \bar{q}_L^\nu \frac{v_u}{\sqrt{2}} \Sigma_R^\nu + M \bar{\Sigma}_L^\nu t_u \Sigma_R^\nu + M \bar{\Sigma}_L^\nu q_R^\nu + h.c. \\ &\quad - \lambda \frac{v_u}{\sqrt{2}} \bar{q}_L^\nu s^{-1} q_R^\nu + h.c. \\ &\quad - \frac{1}{2} q_R^\nu M_{q_R^\nu} q_R^\nu + h.c. , \end{aligned} \quad (\text{A.4})$$

where $M_{q_R^\nu} = \frac{\Lambda_\nu^2}{\Lambda_\nu} \varphi'^T s_\nu^{-1} \varphi'$. The heavy right-chiral neutrino q_R^ν couples to \bar{q}_L^ν both directly and indirectly via $\bar{\Sigma}_L^\nu$ and Σ_R^ν , thereby generating an effective Majorana mass for the left-chiral neutrino \bar{q}_L^ν . Integrating out q_R^ν and $\Sigma_{L,R}^\nu$ in Eq. (A.4) results in

$$\mathcal{L}_{\text{mass}}^\nu = \frac{1}{2} \bar{q}_L^\nu \left[\frac{\Lambda_\nu v_u^2 \lambda^2}{2\Lambda_\varphi^2} (t_u^{-1} + s^{-1}) \varphi'^{-1} s_\nu \varphi'^{-1T} (t_u^{-1} + s^{-1})^T \right] \bar{q}_L^{\nu T} . \quad (\text{A.5})$$

Comparing Eq. (A.5) and Eq. (A.3) we notice two important differences. First, due to its transformation as a $(\mathbf{3}, \bar{\mathbf{3}})$ in flavour space, the matrix φ' contributes non-trivially to the flavour structure of the light neutrinos. Second, the factor $(t_u^{-1} + s^{-1}) \sim Y_u$ features strong hierarchies in contrast to $(\mathbb{1} + s^{-1} t_u)$. These hierarchies must be approximately compensated by an even stronger hierarchy in $M_{q_R^\nu}^{-1}$ in order to generate a phenomenologically viable neutrino mass spectrum. As such a cancellation of hierarchies appears rather ad hoc, we abandon this alternative neutrino extension.

A.2 Charged leptons

As already mentioned in Section 2.3, the structure of the charged lepton Yukawa matrix is identical to the one of the down-type quarks. At the GUT scale we have $Y_e = Y_d$ which is a reasonable approximation. Deviations from this equality can be induced by allowing the flavon fields S or $T^{(\prime)}$ to transform non-trivially under $SU(4)$. Due to their appearance in the Lagrangian of Eq. (2.4), the only alternative representation is the adjoint **15** of $SU(4)$. Such a choice does not alter the quark sector, but it introduces a Georgi-Jarlskog factor of -3 for the leptons [24]. For instance, if S is kept in the singlet representation of $SU(4)$ while $T^{(\prime)}$ furnishes the adjoint representation, we obtain a difference between the Yukawa matrices of the charged leptons and down-type quarks. Explicitly, and adopting the approximation of Section 2.3, we obtain

$$Y_d \sim (s - t')^{-1} + s^{-1}, \quad Y_e \sim (s + 3t')^{-1} + s^{-1}. \quad (\text{A.6})$$

More complicated relations are possible if we allow the flavons S and/or $T^{(\prime)}$ to appear in both $SU(4)$ representations. We conclude that the model can therefore accommodate a viable charged lepton sector as well.

B Determining s and t' numerically

As already discussed in Section 2.3, it is a not-trivial task to invert the relations between the flavour breaking VEVs and the Yukawa matrices. In this Appendix, we present a procedure for calculating s and t' numerically for a given pair of Y_u and Y_d assuming Eq. (2.11) to hold exactly. We therefore write

$$-\frac{1}{\lambda} Y_u = (s + t')^{-1} + s^{-1}, \quad -\frac{1}{\lambda} Y_d = (s - t')^{-1} + s^{-1}. \quad (\text{B.1})$$

Defining $H \equiv s^{-1} t'$ we obtain the expressions

$$-\frac{1}{\lambda} Y_u s = (\mathbb{1} + H)^{-1} + \mathbb{1}, \quad -\frac{1}{\lambda} Y_d s = (\mathbb{1} - H)^{-1} + \mathbb{1}, \quad (\text{B.2})$$

which can be combined to remove the s -dependence

$$G \equiv Y_d Y_u^{-1} = [(\mathbb{1} - H)^{-1} + \mathbb{1}] [(\mathbb{1} + H)^{-1} + \mathbb{1}]^{-1}. \quad (\text{B.3})$$

Let us assume for the moment that G is a triangular matrix, which can always be achieved by a suitable similarity transformation. In that case, also H has a triangular form, so that Eq. (B.3) can be solved explicitly for the six elements of H . We thus obtain an explicit solution for $H(G)$ in the special case of a triangular matrix G .

As $Y_d Y_u^{-1}$ is generally not given in a triangular form, we need to generalize the solution for $H(G)$ to generic forms of G . For this purpose we expand the function $H(G)$ as a series in the matrix G . Due to the Cayley-Hamilton theorem this series stops after the quadratic term.⁹ Hence, we can express $H(G)$ in a basis independent way by

$$H(G) = a \mathbb{1} + b G + c G^2, \quad (\text{B.4})$$

⁹In general the theorem states that for each $n \times n$ matrix M , M^n can be expressed as a polynomial $\sum_{i < n} x_i M^i$, where the factors x_i depend solely on traces of powers of M up to order M^n . For a detailed discussion see e.g. [82, 83].

where the coefficients a , b , and c depend only on the traces of G , G^2 and G^3 . In the special case of a triangular matrix G , it is possible to solve Eq. (B.4) analytically for a , b and c . As these coefficients are basis independent, Eq. (B.4) holds true in any basis; in particular $G = Y_d Y_u^{-1}$ need not be of triangular form.

In principle, we can determine H for a given pair of Yukawa matrices $Y_{u,d}$ analytically. Due to their enormous length, the resulting expressions are however not particularly instructive which is why we content ourselves with a numerical evaluation. Having determined the matrix H , we can use Eq. (B.2) to calculate s

$$s = -\lambda Y_u^{-1} ((\mathbb{1} + H)^{-1} + \mathbb{1}) , \quad (\text{B.5})$$

and the definition of H to determine $t' = s H$. Thus, we have obtained numerical matrices s and t' for a given pair of Yukawa matrices $Y_{u,d}$.

C Diagonalizing the quark mass matrices

In this appendix, we present the technical details related to the diagonalization of the quark mass matrices, discussed in Section 3.1. Starting from the original basis given in Eqs. (3.2,3.3), we perform a sequence of basis transformations to diagonalize \mathcal{M}^u to second order in ϵ_u . The individual intermediate bases are labelled by a subscript (i).

1. Basis with diagonal $s = \hat{s}$:

Thanks to the flavour symmetry $SU(3)_I \times SU(3)_{II}$ we can always choose a basis in which the matrix s is diagonal. $\mathcal{M}_{(1)}^u$ is therefore identical to \mathcal{M}^u of Eq. (3.3) with $s \rightarrow \hat{s}$. Note that this choice of basis is valid for both the up and the down sector.

2. Diagonalizing t_u :

In the second step, we apply the basis transformation

$$\overline{\Psi}_{L(2)}^u \equiv \overline{\Psi}_{L(1)}^u \text{diag}(\mathbb{1}, V_u^\dagger, \mathbb{1}) , \quad \Psi_{R(2)}^u \equiv \text{diag}(V_u, U_u, \mathbb{1}) \Psi_{R(1)}^u , \quad (\text{C.1})$$

to render t_u diagonal, see Eq. (3.5). The resulting mass matrix takes the form

$$\mathcal{M}_{(2)}^u = \begin{pmatrix} 0 & U_u^\dagger \lambda \epsilon_u & \mathbb{1} \\ \mathbb{1} & \hat{t}_u & 0 \\ V_u^\dagger \lambda \epsilon_u & 0 & \hat{s} \end{pmatrix} M . \quad (\text{C.2})$$

Notice that the unitary rotations V_u and U_u reappear at order ϵ_u only. It is furthermore important to realize that the corresponding matrices V_d and U_d for the down sector differ from those of the up sector.

3. Diagonalizing $\mathcal{M}_{(2)}^u$ for $\epsilon_u = 0$:

Setting ϵ_u to zero, the mixing of the three generations disappears completely. Introducing the following cosines and sines,

$$c_s^i = \frac{\hat{s}_i}{\sqrt{1 + \hat{s}_i^2}} , \quad s_s^i = \frac{1}{\sqrt{1 + \hat{s}_i^2}} , \quad c_{t_u}^i = \frac{\hat{t}_u^i}{\sqrt{1 + \hat{t}_u^{i\,2}}} , \quad s_{t_u}^i = \frac{1}{\sqrt{1 + \hat{t}_u^{i\,2}}} , \quad (\text{C.3})$$

we can define the diagonal 3×3 matrices

$$\hat{c}_x = \text{diag}(c_x^1, c_x^2, c_x^3) , \quad \hat{s}_x = \text{diag}(s_x^1, s_x^2, s_x^3) , \quad (\text{C.4})$$

where the index x stands for s or t_u . With this notation at hand, it is straightforward to diagonalize $\mathcal{M}_{(2)}^u$ for $\epsilon_u = 0$. In the basis of

$$\bar{\Psi}_{L(3)}^u \equiv \bar{\Psi}_{L(2)}^u \begin{pmatrix} \hat{c}_s & 0 & \hat{s}_s \\ 0 & \mathbb{1} & 0 \\ -\hat{s}_s & 0 & \hat{c}_s \end{pmatrix} , \quad \Psi_{R(3)}^u \equiv \begin{pmatrix} \hat{c}_{t_u} & -\hat{s}_{t_u} & 0 \\ \hat{s}_{t_u} & \hat{c}_{t_u} & 0 \\ 0 & 0 & \mathbb{1} \end{pmatrix} \Psi_{R(2)}^u , \quad (\text{C.5})$$

the full mass matrix, including the terms proportional to ϵ_u , is given by

$$\mathcal{M}_{(3)}^u = \begin{pmatrix} (-\hat{s}_s V_u^\dagger \hat{c}_{t_u} - \hat{c}_s U_u^\dagger \hat{s}_{t_u}) \lambda \epsilon_u & (-\hat{s}_s V_u^\dagger \hat{s}_{t_u} + \hat{c}_s U_u^\dagger \hat{c}_{t_u}) \lambda \epsilon_u & 0 \\ 0 & \hat{s}_{t_u}^{-1} & 0 \\ (\hat{c}_s V_u^\dagger \hat{c}_{t_u} - \hat{s}_s U_u^\dagger \hat{s}_{t_u}) \lambda \epsilon_u & (\hat{c}_s V_u^\dagger \hat{s}_{t_u} + \hat{s}_s U_u^\dagger \hat{c}_{t_u}) \lambda \epsilon_u & \hat{s}_s^{-1} \end{pmatrix} M . \quad (\text{C.6})$$

Identifying this with the matrix of Eq. (3.6), defines the 3×3 matrices a_u , b_u , c_u , d_u , \hat{e}_u , and \hat{f} . The latter two are diagonal and positive definite.

4. Block-diagonalizing $\mathcal{M}_{(3)}^u$ up to order ϵ_u^2 :

Having parameterized $\mathcal{M}_{(3)}^u$ as in Eq. (3.6), we proceed to block-diagonalize this matrix up to order ϵ_u^2 . To this end, we adopt the following unitary transformations,

$$\bar{\Psi}_{L(4)}^u \equiv \bar{\Psi}_{L(3)}^u [\mathcal{R}_{12}(\xi_{12}^u)]^\dagger [\mathcal{R}_{23}(\xi_{23}^u)]^\dagger [\mathcal{R}_{13}(\xi_{13}^u)]^\dagger , \quad (\text{C.7a})$$

$$\Psi_{R(4)}^u \equiv [\mathcal{R}_{12}(\zeta_{12}^u)] [\mathcal{R}_{23}(\zeta_{23}^u)] [\mathcal{R}_{13}(\zeta_{13}^u)] \Psi_{R(3)}^u , \quad (\text{C.7b})$$

where $\mathcal{R}_{\alpha\beta}(\xi)$ denotes a “rotation in the α - β plane”, expanded to second order in ξ . For $(\alpha, \beta) = (1, 2)$, one has

$$\mathcal{R}_{12}(\xi) = \begin{pmatrix} \mathbb{1} - \frac{1}{2} \xi \xi^\dagger & -\xi & 0 \\ \xi^\dagger & \mathbb{1} - \frac{1}{2} \xi^\dagger \xi & 0 \\ 0 & 0 & \mathbb{1} \end{pmatrix} , \quad (\text{C.8})$$

and the expressions for the other two pairs, (2,3) and (1,3), are identical up to obvious permutations of rows and columns. The matrices ξ and ζ are given in terms of the parameters of Eq. (3.6) by

$$\xi_{12}^u = b_u \hat{e}_u^{-1} \epsilon_u , \quad [\xi_{23}^u]_{ij} = \frac{-\hat{e}_u^i d_u^{\dagger ij}}{\hat{e}_u^{i2} - \hat{f}_j^2} \epsilon_u , \quad \xi_{13}^u = a_u c_u^\dagger \hat{f}^{-2} \epsilon_u^2 , \quad (\text{C.9a})$$

$$\zeta_{12}^u = a_u^\dagger b_u \hat{e}_u^{-2} \epsilon_u^2 , \quad [\zeta_{23}^u]_{ij} = \frac{-d_u^{\dagger ij} \hat{f}_j}{\hat{e}_u^{i2} - \hat{f}_j^2} \epsilon_u , \quad \zeta_{13}^u = c_u^\dagger \hat{f}^{-1} \epsilon_u . \quad (\text{C.9b})$$

We note that the matrices ξ_{23}^u and ζ_{23}^u cannot be written as a simple product of matrices. With a little bit of algebra, it is possible to show that the resulting mass matrix $\mathcal{M}_{(4)}^u$ is given by the matrix in Eq. (3.7).

5. The approximate mass basis:

The final step of the sequence of basis transformations consists in the diagonalization of the upper left 3×3 block of $\mathcal{M}_{(4)}^u$, see Eq. (3.8). The corresponding transformation reads

$$\overline{\Psi}_{L(5)}^u \equiv \overline{\Psi}_{L(4)}^u \text{diag}(\mathcal{V}_u^\dagger, \mathbb{1}, \mathbb{1}) , \quad \Psi_{R(5)}^u \equiv \text{diag}(\mathcal{U}_u, \mathbb{1}, \mathbb{1}) \Psi_{R(4)}^u . \quad (\text{C.10})$$

The basis $\Psi_{L,R(5)}^u$ corresponds to the approximate mass basis denoted by $\Psi_{L,R}^u$ in Section 3.

Applying this sequence of basis transformations to the gauge-kinetic terms changes the \mathcal{K} matrices of Eq. (3.13) to

$$\mathcal{K}_{L(5)}^+ = \begin{pmatrix} \mathcal{V}_u \mathcal{V}_d^\dagger - \mathcal{V}_u \frac{1}{2} (\xi_{12}^u \xi_{12}^{u\dagger} + \xi_{12}^d \xi_{12}^{d\dagger}) \mathcal{V}_d^\dagger & \mathcal{V}_u \xi_{12}^d & -\mathcal{V}_u (\xi_{13}^u - \xi_{13}^d - \xi_{12}^d \xi_{23}^d) \\ \xi_{12}^{u\dagger} \mathcal{V}_d^\dagger & \xi_{12}^{u\dagger} \xi_{12}^d + \xi_{23}^u \xi_{23}^{d\dagger} & -\xi_{23}^u \\ (\xi_{13}^{u\dagger} - \xi_{13}^{d\dagger} + \xi_{23}^{u\dagger} \xi_{12}^{u\dagger}) \mathcal{V}_d^\dagger & -\xi_{23}^{d\dagger} & \mathbb{1} - \frac{1}{2} (\xi_{23}^{u\dagger} \xi_{23}^u + \xi_{23}^{d\dagger} \xi_{23}^d) \end{pmatrix} + \mathcal{O}(\epsilon_{u,d}^3) , \quad (\text{C.11a})$$

$$\mathcal{K}_{R(5)}^+ = \begin{pmatrix} \mathcal{U}_u \zeta_{13}^u \zeta_{13}^{d\dagger} \mathcal{U}_d^\dagger & \mathcal{U}_u \zeta_{13}^u \zeta_{23}^{d\dagger} & -\mathcal{U}_u \zeta_{13}^u \\ \zeta_{23}^u \zeta_{13}^{d\dagger} \mathcal{U}_d^\dagger & \zeta_{23}^u \zeta_{23}^{d\dagger} & -\zeta_{23}^u \\ -\zeta_{13}^{d\dagger} \mathcal{U}_d^\dagger & -\zeta_{23}^{d\dagger} & \mathbb{1} - \frac{1}{2} (\zeta_{13}^{u\dagger} \zeta_{13}^u + \zeta_{23}^{u\dagger} \zeta_{23}^u + \zeta_{13}^{d\dagger} \zeta_{13}^d + \zeta_{23}^{d\dagger} \zeta_{23}^d) \end{pmatrix} + \mathcal{O}(\epsilon_{u,d}^3) , \quad (\text{C.11b})$$

$$\mathcal{K}_{L(5)}^0 = \begin{pmatrix} \mathcal{V} \xi_{12} \xi_{12}^\dagger \mathcal{V}^\dagger & -\mathcal{V} \xi_{12} & -\mathcal{V} \xi_{12} \xi_{23}^\dagger \\ -\xi_{12}^\dagger \mathcal{V}^\dagger & \mathbb{1} - \xi_{12}^\dagger \xi_{12} - \xi_{23} \xi_{23}^\dagger & \xi_{23} \\ -\xi_{23}^\dagger \xi_{12}^\dagger \mathcal{V}^\dagger & \xi_{23}^\dagger & \xi_{23}^\dagger \xi_{23} \end{pmatrix} + \mathcal{O}(\epsilon^3) , \quad (\text{C.11c})$$

$$\mathcal{K}_{R(5)}^0 = \begin{pmatrix} \mathcal{U} \zeta_{13} \zeta_{13}^\dagger \mathcal{U}^\dagger & \mathcal{U} \zeta_{13} \zeta_{23}^\dagger & -\mathcal{U} \zeta_{13} \\ \zeta_{23} \zeta_{13}^\dagger \mathcal{U}^\dagger & \zeta_{23} \zeta_{23}^\dagger & -\zeta_{23} \\ -\zeta_{13}^\dagger \mathcal{U}^\dagger & -\zeta_{23}^\dagger & \mathbb{1} - \zeta_{13}^\dagger \zeta_{13} + \zeta_{23}^\dagger \zeta_{23} \end{pmatrix} + \mathcal{O}(\epsilon^3) . \quad (\text{C.11d})$$

As the basis transformations depend on the isospin components, we have labelled the resulting flavour structures by superscripts which indicate whether they relate to charged or neutral currents. In the latter case, we have suppressed the isospin indices for convenience. Note that $\mathcal{K}_{R(5)}^0$ can be derived from $\mathcal{K}_{R(5)}^+$ by dropping the indices u and d .

References

- [1] A. J. Buras, J. R. Ellis, M. K. Gaillard and D. V. Nanopoulos, Nucl. Phys. B **135** (1978) 66.
- [2] H. Fritzsch and P. Minkowski, Annals Phys. **93** (1975) 193.
- [3] P. Minkowski, Phys. Lett. B **67** (1977) 421.
- [4] M. Gell-Mann, P. Ramond and R. Slansky, Conf. Proc. C **790927** (1979) 315 [arXiv:1306.4669].

- [5] T. Yanagida, Conf. Proc. C **7902131** (1979) 95.
- [6] R. N. Mohapatra and G. Senjanovic, Phys. Rev. Lett. **44** (1980) 912.
- [7] H. Georgi and S. L. Glashow, Phys. Rev. Lett. **32** (1974) 438.
- [8] J. C. Pati and A. Salam, Phys. Rev. D **8** (1973) 1240.
- [9] J. C. Pati and A. Salam, Phys. Rev. D **10** (1974) 275 [Phys. Rev. D **11** (1975) 703].
- [10] F. Hartmann, W. Kilian and K. Schnitter, JHEP **1405** (2014) 064 [arXiv:1401.7891].
- [11] W. Kilian and J. Reuter, Phys. Lett. B **642** (2006) 81 [hep-ph/0606277].
- [12] R. Howl and S. F. King, Phys. Lett. B **652** (2007) 331 [arXiv:0705.0301].
- [13] L. Calibbi, L. Ferretti, A. Romanino and R. Ziegler, Phys. Lett. B **672** (2009) 152 [arXiv:0812.0342].
- [14] F. Braam, J. Reuter and D. Wiesler, AIP Conf. Proc. **1200** (2010) 458 [arXiv:0909.3081].
- [15] V. De Romeri, M. Hirsch and M. Malinsky, Phys. Rev. D **84** (2011) 053012 [arXiv:1107.3412].
- [16] C. Arbelaez, R. M. Fonseca, M. Hirsch and J. C. Romao, Phys. Rev. D **87** (2013) 7, 075010 [arXiv:1301.6085].
- [17] C. Arbeláez, M. Hirsch, M. Malinský and J. C. Romão, Phys. Rev. D **89** (2014) 3, 035002 [arXiv:1311.3228].
- [18] M. C. Chen and K. T. Mahanthappa, Int. J. Mod. Phys. A **18** (2003) 5819 [hep-ph/0305088].
- [19] S. F. King, Rept. Prog. Phys. **67** (2004) 107 [hep-ph/0310204].
- [20] R. N. Mohapatra and A. Y. Smirnov, Ann. Rev. Nucl. Part. Sci. **56** (2006) 569 [hep-ph/0603118].
- [21] G. Altarelli and F. Feruglio, Rev. Mod. Phys. **82** (2010) 2701 [arXiv:1002.0211].
- [22] S. F. King and C. Luhn, Rept. Prog. Phys. **76** (2013) 056201 [arXiv:1301.1340].
- [23] S. F. King, A. Merle, S. Morisi, Y. Shimizu and M. Tanimoto, New J. Phys. **16** (2014) 045018 [arXiv:1402.4271].
- [24] H. Georgi and C. Jarlskog, Phys. Lett. B **86** (1979) 297.
- [25] S. Antusch and M. Spinrath, Phys. Rev. D **79** (2009) 095004 [arXiv:0902.4644].
- [26] C. D. Froggatt and H. B. Nielsen, Nucl. Phys. B **147** (1979) 277.

- [27] M. Leurer, Y. Nir and N. Seiberg, Nucl. Phys. B **398** (1993) 319 [hep-ph/9212278].
- [28] M. Leurer, Y. Nir and N. Seiberg, Nucl. Phys. B **420** (1994) 468 [hep-ph/9310320].
- [29] S. F. King and G. G. Ross, Phys. Lett. B **574** (2003) 239 [hep-ph/0307190].
- [30] S. F. King and M. Malinsky, JHEP **0611** (2006) 071 [hep-ph/0608021].
- [31] S. F. King and M. Malinsky, Phys. Lett. B **645** (2007) 351 [hep-ph/0610250].
- [32] S. F. King and C. Luhn, Nucl. Phys. B **820** (2009) 269 [arXiv:0905.1686].
- [33] B. Dutta, Y. Mimura and R. N. Mohapatra, JHEP **1005** (2010) 034 [arXiv:0911.2242].
- [34] S. F. King and C. Luhn, Nucl. Phys. B **832** (2010) 414 [arXiv:0912.1344].
- [35] R. de Adelhart Toorop, F. Bazzocchi and L. Merlo, JHEP **1008** (2010) 001 [arXiv:1003.4502].
- [36] I. de Medeiros Varzielas, JHEP **1201** (2012) 097 [arXiv:1111.3952].
- [37] F. Hartmann and W. Kilian, Eur. Phys. J. C **74** (2014) 3055 [arXiv:1405.1901].
- [38] S. F. King, JHEP **1408** (2014) 130 [arXiv:1406.7005].
- [39] B. Grinstein, M. Redi and G. Villadoro, JHEP **1011** (2010) 067 [arXiv:1009.2049].
- [40] M. E. Albrecht, T. Feldmann and T. Mannel, JHEP **1010** (2010) 089 [arXiv:1002.4798].
- [41] T. Feldmann, M. Jung and T. Mannel, Phys. Rev. D **80** (2009) 033003 [arXiv:0906.1523].
- [42] R. Alonso, M. B. Gavela, L. Merlo and S. Rigolin, JHEP **1107** (2011) 012 [arXiv:1103.2915].
- [43] E. Nardi, Phys. Rev. D **84** (2011) 036008 [arXiv:1105.1770].
- [44] R. Alonso, M. B. Gavela, D. Hernandez and L. Merlo, Phys. Lett. B **715** (2012) 194 [arXiv:1206.3167].
- [45] J. R. Espinosa, C. S. Fong and E. Nardi, JHEP **1302** (2013) 137 [arXiv:1211.6428].
- [46] R. Alonso, M. B. Gavela, D. Hernández, L. Merlo and S. Rigolin, JHEP **1308** (2013) 069 [arXiv:1306.5922].
- [47] R. Alonso, M. B. Gavela, G. Isidori and L. Maiani, JHEP **1311** (2013) 187 [arXiv:1306.5927].
- [48] R. Alonso de Pablo, arXiv:1307.1904.

- [49] C. S. Fong and E. Nardi, Phys. Rev. D **89** (2014) 3, 036008 [arXiv:1307.4412].
- [50] L. Merlo, arXiv:1503.03282.
- [51] A. J. Buras, M. V. Carlucci, L. Merlo and E. Stamou, JHEP **1203** (2012) 088 [arXiv:1112.4477].
- [52] R. T. D’Agnolo and D. M. Straub, JHEP **1205** (2012) 034 [arXiv:1202.4759].
- [53] T. Feldmann, JHEP **1104** (2011) 043 [arXiv:1010.2116].
- [54] D. Guadagnoli, R. N. Mohapatra and I. Sung, JHEP **1104** (2011) 093 [arXiv:1103.4170].
- [55] R. N. Mohapatra, AIP Conf. Proc. **1467** (2012) 7 [arXiv:1205.6190].
- [56] G. Krnjaic and D. Stolarski, JHEP **1304** (2013) 064 [arXiv:1212.4860].
- [57] R. Franceschini and R. N. Mohapatra, JHEP **1304** (2013) 098 [arXiv:1301.3637].
- [58] R. N. Mohapatra and J. W. F. Valle, Phys. Rev. D **34** (1986) 1642.
- [59] R. Slansky, Phys. Rept. **79** (1981) 1.
- [60] R. S. Chivukula and H. Georgi, Phys. Lett. B **188** (1987) 99.
- [61] L. J. Hall and L. Randall, Phys. Rev. Lett. **65** (1990) 2939.
- [62] A. J. Buras, P. Gambino, M. Gorbahn, S. Jäger and L. Silvestrini, Phys. Lett. B **500** (2001) 161 [hep-ph/0007085].
- [63] G. D’Ambrosio, G. F. Giudice, G. Isidori and A. Strumia, Nucl. Phys. B **645** (2002) 155 [hep-ph/0207036].
- [64] V. Cirigliano, B. Grinstein, G. Isidori and M. B. Wise, Nucl. Phys. B **728** (2005) 121 [hep-ph/0507001].
- [65] W. Büchmüller and D. Wyler, Nucl. Phys. B **268** (1986) 621.
- [66] K. A. Olive *et al.* [Particle Data Group Collaboration], Chin. Phys. C **38** (2014) 090001.
- [67] Z. Z. Xing, H. Zhang and S. Zhou, Phys. Rev. D **77** (2008) 113016 [arXiv:0712.1419].
- [68] M. Bona *et al.* [UTfit Collaboration], JHEP **0610** (2006) 081 [hep-ph/0606167].
- [69] J. Charles *et al.* [CKMfitter Group Collaboration], Eur. Phys. J. C **41** (2005) 1 [hep-ph/0406184].
- [70] A. J. Bevan *et al.* [BaBar and Belle Collaborations], Eur. Phys. J. C **74** (2014) 11, 3026 [arXiv:1406.6311].

- [71] A. J. Buras, K. Gemmler and G. Isidori, Nucl. Phys. B **843** (2011) 107 [arXiv:1007.1993].
- [72] A. Crivellin and S. Pokorski, Phys. Rev. Lett. **114** (2015) 1, 011802 [arXiv:1407.1320].
- [73] T. Feldmann, B. Müller and D. van Dyk, arXiv:1503.09063.
- [74] R. Röntsch and M. Schulze, JHEP **1407** (2014) 091 [arXiv:1404.1005].
- [75] R. Röntsch and M. Schulze, arXiv:1501.05939.
- [76] S. Schael *et al.* [ALEPH and DELPHI and L3 and OPAL and SLD and LEP Electroweak Working Group and SLD Electroweak Group and SLD Heavy Flavour Group Collaborations], Phys. Rept. **427** (2006) 257 [hep-ex/0509008].
- [77] P. P. Giardino, K. Kannike, I. Masina, M. Raidal and A. Strumia, JHEP **1405** (2014) 046 [arXiv:1303.3570].
- [78] D. López-Val, T. Plehn and M. Rauch, JHEP **1310** (2013) 134 [arXiv:1308.1979].
- [79] T. Corbett, O. J. P. Eboli, D. Goncalves, J. Gonzalez-Fraile, T. Plehn and M. Rauch, arXiv:1505.05516.
- [80] V. Khachatryan *et al.* [CMS Collaboration], JHEP **1409** (2014) 087 [JHEP **1410** (2014) 106] [arXiv:1408.1682].
- [81] G. Aad *et al.* [ATLAS Collaboration], arXiv:1503.05066.
- [82] F. Zhang, *Matrix theory: basic results and techniques*, Springer (2011).
- [83] P. Petersen, *Linear algebra*, Springer (2012).